USP18 is an essential regulator of muscle cell differentiation and maturation

Cyriel Sebastiaan Olie[1], Adán Pinto-Fernández[2,3], Andreas Damianou[2,3], Salma el Abdellaoui[1], Iolanda Vendrell[2,3], Hailiang Mei[4], Bianca den Hamer[1], Erik van der Wal[1], Jessica C. de Greef[1], Anneke J. van der Kooi[5],Joost Raaphorst[5], Eleonora Aronica[6], Vered Raz[1*] and Benedikt M. Kessler[2,3*]

[1]Human Genetics department, Leiden University Medical Centre, 2333ZC Leiden, The Netherlands.

[2]Chinese Academy for Medical Sciences Oxford Institute, Nuffield Department of Medicine, University of Oxford, Roosevelt Drive, Oxford OX3 7FZ, UK

[3]Target Discovery Institute, Centre for Medicines Discovery, Nuffield Department of Medicine, University of Oxford, Oxford, OX3 7FZ, UK

[4]Sequencing Analysis Support Core, Leiden University Medical Centre, 2333ZC Leiden, The Netherlands.

[5]Department of Neurology, Amsterdam University Medical Centre, location AMC, Amsterdam Neuroscience Institute, Amsterdam, The Netherlands

[6]Department of Neuropathology, Amsterdam University Medical Centre, The Netherlands

*To whom correspondence should be addressed. v.raz@lumc.nl, Tel: +31-715269488; benedikt.kessler@ndm.ox.ac.uk, Tel: +44-1865612921

Running Title: USP18 regulates muscle cell differentiation and maturation

Abstract
USP18 negatively regulates the IFN-1 signalling pathway by removing ISG15, a di-ubiquitin analogue, from substrate proteins and plays a role in immune related pathologies. Dermatomyositis (DM), a rare muscle degeneration disease, is characterised by an excessive immune response and IFN-1 signaling. In DM muscles we found USP18 expression within myofibers at regenerating regions, suggesting a role in muscle cell biology. Surprisingly, we observed that USP18 depletion induced muscle cell differentiation under nutrient-rich conditions. USP18 expression and function was independent of ISG15 and IFN-1 signalling, but concomitant with reduced cell cycle and sarcomeric gene networks. USP18 depletion let to altered expression of myogenic (co-)transcription factors, indicating that USP18 tightly regulates the muscle cell differentiation program. Moreover, USP18-depletion impacted physiological features in differentiated muscle cells, suggesting a role in differentiation maintenance. Our results revealed USP18 as a critical regulator of multiple steps during muscle cell differentiation independent of the IFN-1 pathway.

Introduction

Idiopathic inflammatory myopathies (myositis) are rare autoimmune diseases that lead to progressive muscle weakness. The molecular mechanisms contributing to myositis pathology are still largely unknown (*1*). Activated interferon (IFN) pathways appear to be a major hallmark, potentially playing an important role in the pathophysiology of myositis. However, the IFN subtypes involved, and their molecular mechanisms, differ between myositis subsets (*2*). Dermatomyositis (DM) is the most frequent type of myositis (incidence of 1:100,000), which is characterised by excessive activation of the interferon type-1 (IFN-1) pathway (*3-5*). The IFN-1 pathway is typically activated upon viral or bacterial infections (*6*). Yet, a link between microbial pathogenesis and DM, for instance as a consequence of SARS CoV-2 infection or other viruses, appears to be rare and therefore not the most common cause (*7, 8*).

Activation of the IFN-1 pathway in response to extracellular threats leads to *de novo* expression of interferon-stimulated genes (ISGs) including ISG15, a ubiquitin-like protein (ubl), and its subsequent conjugation to substrate proteins (ISGylation) (*9*). ISGylation, in analogy to ubiquitination, can affect protein stability or localization and thereby alter cellular processes, such as protein translation (*10*), DNA repair (*11*), innate immune (*12, 13*) and antiviral responses (*14, 15*). IFN-1 stimulation also leads to expression of USP18 (UBP43), a cysteine protease that removes conjugated ISG15 from substrate proteins (de-ISGylation) (*16*). In addition, independent of its enzymatic activity, USP18 can inhibit IFN-1 signal transduction by binding the Interferon-alpha/beta receptor (IFNAR2) (*17*). USP18 deficiency causes interferonopathies in mice and humans (*18-20*). Furthermore, USP18 appears to be involved in tumorigenesis by affecting several cellular signalling pathways (*21-23*), although the exact molecular mechanisms are less clear.

In DM, USP18 and ISG15 expression levels are substantially increased (+60- and +300- folds, respectively) as compared to other inflammatory myopathies (*24*). Despite the increase in USP18 expression, a prominent accumulation of ISG15-conjugated proteins was observed, concomitant with a lower abundance of sarcomeric proteins in atrophic myofibers in the perifascicular regions of DM compared to healthy muscles (*4, 24*). The role of USP18 in DM pathology is largely unknown. We investigated USP18 expression in DM muscles and report a marked expression of USP18 with regenerating myofibers. We then investigated USP18's role in muscle cell biology and provide evidence that USP18 acts a novel regulator of muscle cell differentiation independent of IFN-1.

Results

Dermatomyositis characterised by muscle degeneration suggest a role for USP18 in muscle regeneration.

To explore USP18 expression in DM muscles, we compared USP18 and ISG15 spatial localization. Consistent with a previous study (*3*), ISG15 signal was found in myofibers close to perifascicular regions (Fig. S1A). Sequential cross-sections showed that the ISG15-positive myofibers were also positive for USP18 (Fig. 1A and S1A). Yet, ISG15 was not always found in USP18-positive myofibers (Fig. 1A and S1A). USP18-positive myofibers were, in part, centrally nucleated (Fig. 1A and S1A). Central nucleation and embryonic Myosin heavy chain (eMyHC) mark regenerating myofibers (*25*). USP18-positive myofibers did not overlap with eMyHC, instead they were found to be neighbouring to eMyHC positive myofibers (Fig. 1A and S1A). Since eMyHC marks newly forming myofibers but not maturing myofibers, we investigated USP18 spatiotemporal expression throughout degeneration and regeneration after cardiotoxin injection into mouse gastrocnemius muscles. The expression of eMyHC was found at four days after injection and reduced at eight days after injection (Fig. 1B). USP18 signal was already found at two days after injection, colocalized with eMyHC positive cells at four days after injection and remained high at eight days after injection where it was found in centrally nucleated myofibers (Fig. 1B and 1C). Together, these observations demonstrate that USP18 is specifically localized in regenerating regions and raise the hypothesis that USP18 could play a role in muscle regeneration.

USP18 depletion causes muscle cell differentiation.

Muscle regeneration is modelled in cell culture by serum starvation, forcing cells to stop proliferating and fuse into multinucleated cells, called myotubes. This is a multistep process that is transcriptionally regulated by myogenic factors (*26*). Mature myotubes were formed after three days of starvation (differentiation). USP18 levels gradually increased during muscle cell differentiation (Fig. 2A), preceding the expression of MyHC (Fig. 2B). To explore whether USP18 plays a role in muscle cell differentiation, we knocked down USP18 expression using three siRNAs (Fig. 2C and S2). USP18 knockdown (KD) in proliferating cultures was confirmed by IFN-1 treatment since endogenous USP18 levels were below detection level (Fig. 2D and S2D). Notably, depletion of USP18, with all three siRNAs, triggered muscle cell differentiation regardless of starvation stress (Fig. 2C-D, Fig. S2). Subsequent experiments were performed with the siRNA-C.

Muscle cell fusion highly dependents on cell density (*27*). Notably, in the USP18-depleted cell cultures, higher fusion was found despite reduced cell number, as compared to control cultures (Fig. 2E). A cell density analysis showed that USP18 depleted cultures did not reach 100% confluency as observed in control cultures

(Fig. S3), suggesting reduced proliferation, which agrees with USP18 regulation of cell proliferation (*21, 28*). Prolonged incubation of USP18-depleted cells in proliferation medium, 72 instead of 24 hours, resulted in a 3-fold increase in fusion index compared to control proliferating cultures (Fig. 2E-G). Notably, prolonged incubation in differentiation medium led to detachment of fully differentiated cells in USP18-depleted cultures, whereas control cultures fully differentiated during 72 hour starvation (Fig. 2F-G). A western blot analysis of protein extracts from still attached versus detached cells floating in the differentiation medium after 72 hour incubation showed an increase in MyHC in the detached fraction and decrease in attached fraction compared to control cells (Fig. 2H-I). This confirmed the detachment of myotubes in USP18-depleted cultures. Together, these results suggest that USP18 may play a dual role during muscle cell differentiation. First, it operates as a molecular "block" at the interface between cell proliferation and initiation of differentiation and at a later step of differentiation, USP18 may regulate maintenance of the fully differentiated cells (Fig. 2J).

USP18-mediated muscle cell differentiation is independent of IFN-1 and deISGylation.

We next investigated whether increased USP18 expression during differentiation was regulated by the IFN-1 pathway. If the IFN-1 pathway is activated, we expect to find upregulation of Interferon stimulated genes (ISGs). However, expression levels of 23 ISGs, except USP18, were unchanged or significantly downregulated in cell cultures after 24 hours of differentiation (Fig. 3A, Table S3). Moreover, the expression of intrinsic cytokines (*IFN-1-α/β*) that activate the IFN-1 pathway were not detected, and their regulatory factor (*IRF7*) was unchanged (Fig. 3B, Table S3). Together, this indicated that during muscle cell differentiation, *USP18* expression is induced independently of the IFN-1 pathway (Fig. 3B). In agreement with previous studies (*29-31*), we also found that IFN-1 treatment reduced muscle cell fusion (Fig. S4), further supporting an IFN-1-independent role for USP18 during muscle cell differentiation.

As USP18 is known to cleave ISG15 from substrate proteins (*32*), we reasoned that an increase in USP18 during muscle cell differentiation could still lead to a reduction of intrinsic ISG15 conjugation to substrate proteins. However, increased USP18 levels during differentiation were not found to be concomitant with changes in ISG15-conjugation (Fig. 3C). To further assess whether differentiation in USP18-depleted cultures might be dependent on ISG15, we knocked down ISG15 expression using siRNA as reported (*12, 33*). ISG15 and ISG15+USP18 KD was confirmed after IFN-1 treatment since ISG15 protein levels were below western blot detection level under proliferating conditions (Fig. 3D). ISG15 KD did not induce differentiation and ISG15 KD did also not prevent differentiation driven by USP18 depletion (Fig. 3E). This

demonstrates that USP18 regulates muscle cell differentiation independent of ISG15. To further confirm this, we repeated the experiments in a human muscle progenitor cell line. Also in the muscle progenitor line, USP18 depletion induced differentiation independent of ISG15 (Fig. S5). Moreover, differentiation in USP18 KD cell cultures did not dependent on serum-starvation, and in control cells USP18 levels also increased during differentiation (Fig. S5). Together, these data indicate that the USP18-dependent switch between proliferation and differentiation is independent of ISG15 and (de-)ISGylation.

USP18 depletion impacts the global myogenic differentiation program.
To elucidate the molecular pathways that are associated with USP18 dependent regulation of muscle cell differentiation, mRNA sequencing was performed on USP18-depleted cells that were cultured for 24 hours in proliferation or differentiation medium. USP18 KD led to massive statistically significant ($p<0.05$, FDR) changes in mRNA expression levels from which, 1445 genes pass the FC>|2| cut off (Fig. 4A). To identify expression patterns that are affected by USP18 levels, we employed hierarchical clustering on the most affected genes (FC>|4|, N=509). Four prominent clusters were found. The pattern of the largest cluster (IV, 276 genes) followed *USP18* expression levels (Fig. 4B). Cluster IV was significantly enriched with the cell cycle gene network (FDR = $3x10^{-68}$) (Fig. 4C). Cluster I, 80 genes, showed an opposite pattern to cluster IV, an increased gene expression in USP18-depleted cultures as compared to control (Fig. 4B). This cluster (I) was enriched with genes encoding for proteins of the extracellular matrix (ECM), calcium channels and the G-protein coupled receptors (GPCR) (Fig. 4C). Cluster III included 132 genes whose expression increased in differentiating cell cultures, control or USP18 KD (Fig. 4B). This cluster was enriched with genes encoding for muscle contraction proteins, GPCR, and calcium channel networks (Fig. 4C). In contrast to cluster III, Cluster II (N=21) showed that USP18 depletion prevented an increase in myosin filament network genes, which is normally observed during muscle cell differentiation (Fig. 4B-C, Table 3). Indeed, a comparison of differentiated cultures between USP18 KD and controls showed that the vast majority of significantly affected muscle-specific genes were reduced by USP18 KD (Fig. 4D). Together, this suggests that the differentiated muscle cells in USP18 KD cultures molecularly differ from the control differentiated cells.

Muscle cell differentiation is transcriptionally regulated by myogenic regulatory factors (MRFs) and myocyte enhancing factors (MEFs) (*26, 34*). We examined their expression levels to elucidate the USP18-dependent effect on muscle cell differentiation. *MYOG* levels were highly upregulated in USP18-depleted cells cultured in proliferation medium (Fig. 4E), which is consistent with the fact that *MYOG* expression drives muscle cell differentiation (*35*). High *MYOD* expression is essential for proliferation of muscle cells and is reduced as terminal differentiation via

increased *MYOG* occurs (*36*). USP18 depleted cells cultured in proliferation medium showed a reduction in *MYOD1* (Fig. 4E), which is normally not observed during early differentiation in our cells (Fig. S6). Together, this could indicate that the differentiation program in USP18-depleted cultures is accelerated compared to control differentiated cultures. Nevertheless, *MYOG* and *MYOD1* levels in serum-starvation conditions were only minorly affected by USP18 depletion (Fig. 4E). Most strikingly, *MEF2A* expression levels, normally increased during differentiation, remained unchanged in USP18 KD driven differentiation regardless of starvation (Fig. 4E and S6). Notably, the *MEF2C* and *-2D* isoforms consistently increased during normal differentiation and USP18 KD driven differentiation (Table S3). This suggests that from the MEF2 gene family, USP18 specifically regulates *MEF2A*. In USP18 KD cell cultures, *MYF5* and *MYF6* levels showed only minor differences compared with control cells (Fig. 4E). RT-qPCR for a subset of these genes validated the RNAseq analysis (Fig. S6). Taken together, we suggest that differentiation driven by USP18 depletion, occurs via transcription regulation of MYOG and MEF2A (Fig. 4F).

We then examined the USP18-dependent proteome to elucidate the consequences of the altered transcriptional differentiation program. Since only ~10% of cells were differentiated after 24 hours (Fig. 2E), possible changes might be masked within the global muscle cell proteomic profiles. Therefore, we selected a 0.25 FDR correction as a cut off (Fig. 5A) and validated this FDR threshold with western blotting (Fig. 5B). USP18 depletion resulted in 40 proteins to significantly decrease and 23 to increase compared to control differentiated cultures (Fig. 5A, Table S4). Protein-protein interaction network analysis revealed a USP18 KD-dependent increase in the muscle-specific cluster (Fig. 5C). To identify expression trends that are associated with USP18 KD-driven differentiation, hierarchical clustering was performed on all significantly affected proteins (N=117, Table S4). Five distinctive clusters were found of which the largest cluster (B) consisted of 41 proteins that increased in starved control and USP18 depleted cultures (Fig. 5D). 11 proteins were annotated to the muscle network (Fig. 5E), of which nine proteins were found back in the RNA cluster III (Fig. 4B). The opposite expression profiles, decreased expression in both starved control and USP18 depleted cultures, were found in cluster A (N=21). Seven proteins from that cluster were found to be part of the DNA replication network (Fig. 5E), of which six were overlapping with RNA cluster IV (Fig. 4B-C). Cluster D consisted of 28 proteins that were increased in differentiated control cultures but were unchanged in USP18 KD differentiated cultures (Fig. 5D). The expression profiles of cluster C and E showed a steep increase or decrease in USP18 KD differentiated cells as compared to controls (Fig. 5D). Protein-protein interaction network analysis on the 117 significantly affected proteins showed that the muscle proteins, DNA replication, and the mitochondria were the most affected networks (Fig. 5E). Next, we directly compared gene to protein fold changes and found a more pronounced change on

protein levels (Fig. 5F). However, only two out of the 21 significantly reduced muscle genes were detected at the protein level, which is most likely due to the short time frame of differentiation (24h) and reduced transcript levels.

***In vitro* muscle maturation is disrupted in absence of USP18.**

Since sarcomere network and calcium channels were amongst the components found to be strongly affected by USP18 KD, we hypothesised that contraction might be impacted. To test this, an USP18-dependent impact on the calcium flux was assessed in mature, multinucleated, fused muscle cells. In control cultures, multinucleated cells showed a strong calcium flux, whereas calcium flux was not detected in undifferentiated cells (Fig. S7). Calcium flux in cell cultures transfected with siControl was indifferent from parental cell culture counterparts (Fig. 6B and S7). In USP18-depleted cultures, the multinucleated cells that were formed in proliferation medium showed a strong calcium flux as compared to undifferentiated cells (Fig. 6A-B). In contrast, a calcium flux was not detected in USP18 KD multinucleated cells that were formed in differentiating medium (Fig. 6A-B). We then investigated the effect of USP18 on muscle contraction in 3D muscle bundles. Intact muscle bundles were formed after siRNA transfection (siControl or siUSP18, Fig. 6C). In USP18 KD muscle bundles, both twitch and tetanic contractile forces were strongly reduced compared to control siRNA muscle bundles (Fig. 6D). USP18 KD in the muscle bundle was confirmed using RT-qPCR (Fig. 6E). The structural integrity of the muscle bundles was assessed by staining for titin. In USP18 KD muscle bundles a clear disruption in myofibers continuity was found compared to control muscle bundles (Fig. 6F). Moreover, a very weak striated titin staining was found in USP18-depleted myofibers compared to controls, indicating sarcomeric disruption (Fig. 6F). This suggests that muscle fibers are formed but not maintained, which is consistent with USP18 KD-mediated detachment of fully differentiated cells in 2D cultures (Fig. 2F-H).

Discussion

The role of USP18 has predominantly been studied in the context of IFN-1 related immune responses, relevant for viral or bacterial infections and the immunogenicity of cancer cells (*6, 12*). Activation of the IFN-1 pathway induces USP18 expression, which in turn modulates the IFN-1 immune response. USP18 deficiency in patients is lethal during the perinatal period, in part due to excessive uncontrolled IFN-1 immune responses that predominantly affect the central nervous system (*19*). A case report suggested that immunosuppressors can rescue the patient's life (*18*). Excessive IFN-1 signalling is also found in some inflammatory myopathies, where muscle degeneration hampers mobility. Although treatments blocking or attenuating the immune response seems beneficial for patients with inflammatory myopathies (*4, 37, 38*), restoring muscle degeneration requires understanding of the molecular mechanisms in affected myofibers. Whereas USP18 is classically found to be expressed in the context of IFN-1 signalling, here we show that this may not be the case during muscle cell differentiation. Depletion of USP18 revealed an important role during muscle cell differentiation, which, together with a marked USP18 localization at regenerating regions, suggest an IFN-1-independent regulatory role for USP18 in muscle biology. So far, a muscle-specific phenotype has not been noted in USP18-deficient patients and USP18 KO mouse models, which are mainly dominated by sarcoma formation, impaired development or lethality (*39-41*).

In the context of IFN-1 signalling, USP18 blocks the interaction between the IFN-1 receptor and downstream effectors as well as regulates ISG15 deconjugation (deISGylation). Consistent with this, deletion of USP18 increases ISGylation of cell cycle regulators that ultimately contribute to cell cycle arrest (*21, 28, 42, 43*). In contrast, we observed that USP18 depletion in muscle cells stopped cellular proliferation, but ISGylation was not found to be involved. Furthermore, ISG15 KD did also not prevent USP18 KD-mediated induction of differentiation. Similarly, ISG15 KD did not affect myotube formation in mouse C2C12 cells (*30*). ISGylation was shown to affect protein turnover (*44*). Yet, in our study, USP18 depletion led to a genome-wide impact on gene expression profiles. This suggests that USP18 regulates muscle cell differentiation via the myogenic transcription program, rather than via its classical function of regulating ISGylation. Consistent with an ISG15-independent function of USP18 in muscle cells, morphological abnormalities were not found in USP18 C64A catalytically inactive knock-in mice, thereby supporting a non-canonical mechanism (*15, 45*).

Muscle cell differentiation is a multi-step program characterised by temporal changes of myogenic (co-)transcription factor levels regulating the expression of muscle structural proteins (*26*). These structural proteins are essential for forming and maintaining myofiber integrity and for facilitating contraction (*46*). Moreover, aberrant

architecture of muscle structural genes leads to reduced cell fusion (*47*). The differentiation process of USP18-depleted cultures was characterised by a reduction of muscle structural genes. In addition, we also show that USP18-depletion leads to reduced contraction in a muscle bundle model. Specifically, we showed that myofiber and sarcomeric integrity were impacted by reduced USP18 levels. Among the sarcomeric genes, *MYOM1* levels were strongly reduced in USP18 KD cultures. MYOM1 is essential for sarcomere stability and thereby crucial for contraction (*48*). For instance, KO of MYOM1 in cardiomyocytes was found to impair calcium homeostasis together with reduced contraction (*49*). Similarly, in USP18-depleted fused cells, calcium influx was found to be impaired. Together, our results suggest that USP18 initially blocks entry into differentiation and subsequently regulates the expression of proteins that form and maintain mature myofibers (Fig. 2J and 6G).

Initial steps in the myogenic transcription program include a decrease in *MYF5* and an increase in *MEF2* isoforms and *MYOG*. Interestingly, USP18 KD driven differentiation was also characterised by decreased *MYF5* and increased *MYOG*, but KD of USP18 specifically prevented an increase of *MEF2A*, but not the *-2C* and *-2D* isoforms. MEF2A is an essential co-transcriptional regulator of muscle cell differentiation (*34*). *MYOM1* and other reduced muscle-specific genes, such as *MYH7*, are directly regulated by MEF2A, which were found to decrease upon USP18 depletion (*50, 51*). Moreover, a MEF2A KD was also described to affect calcium homeostasis in C2C12 cells and has also been described to regulate the cell cycle and differentiation of cardiomyocytes (*34, 50, 51*). How USP18 is upregulated during muscle cell differentiation remains obscure. KD of the upstream regulators of USP18, such as JAK/STAT1, has also been shown to increase differentiation via elevating levels of MEF2 and MYOG (*52*). We show that the MEF2A isoform levels are specificity affected by USP18, whether USP18 regulation of MEF2A impacts maturation were not explored (*52*).

Based on our results showing that USP18's role in muscle cell differentiation appears to be independent of IFN-1. Therefore, we suggest that USP18 molecular function in the inflammatory system might be different compared to myogenesis and regeneration. In acute injured skeletal muscles, inflammation precedes removal of damaged tissue, which subsequently triggering regeneration via the secretion of cytokines, such as IFN-γ and TNF-α (*53-55*). Yet, excessive inflammation in DM is linked to muscle degeneration. An interplay between the USP18 IFN-1-dependent function, de-ISGylation, and the USP18 IFN-1-independent role in regeneration is challenging to study. DM is multifactorial pathology and progression should be studied in longitudinal muscle biopsies. Moreover, modelling inflammation in muscle cell culture also remains a challenge, but to test the hypothesis of a role in inflammation versus regeneration, muscle bundle cultures could be combined with inflammatory cells (*56*). This, together with DM derived muscle cells, might present a

relevant model to further explore an IFN-1 independent role for USP18, providing the framework for specific therapies.

Taken together, our study shows that USP18's function is broader that the IFN-1 pathway and the immune system. We show that USP18 regulates muscle cell differentiation independent of (de)ISGylation and the IFN-1 pathway. USP18 depletion causes muscle cells to switch from proliferation to entering differentiation irrespective of starvation. USP18 also plays a role in maturation, ensuring proper expression of sarcomeric genes. These effects appear to be irrespective of USP18-dependent deISGylation. We suggest that a USP18 IFN-1-independent pathway may contribute to muscle regeneration in muscle pathologies. Future research will have to pinpoint the exact mechanism by which USP18 is induced and how USP18 subsequently regulates the transcriptional regulators of muscle cell differentiation.

Methods

Human muscle sample collection

Biopsies from deltoid (2x) or vastus lateralis (1x) muscle were obtained as left-over material from three patients that were diagnosed with dermatomyositis (DM) according to the clinico-morphological European Neuromuscular Centre criteria (*57*). Biopsies were immediately snap-frozen in liquid nitrogen and stored at -80°C for further analyses.

Mouse muscle

Male mice of 2 months old (C57BL/10ScSnJ strain) were injected in the left and right gastrocnemius with 50 µl cardiotoxin (CTX; 10µM) after being anaesthetized with isoflurane, according to approved research protocol (DEC: # 13141, LUMC, Leiden, The Netherlands). Mice (N=1 per group) were sacrificed either without injection (day 0 = control) or 2, 4 or 8 days after the CTX injection. Gastrocnemius muscles were collected and snap-frozen in liquid nitrogen cooled isopentane and subsequently stored in -80 °C.

Cryosectioning and tissue staining.

Sectioning of both human and mouse muscles was performed using the cryostat at 10 µm thickness (Leica, Solms, Germany). Cross sections of the mice muscles were taken in the middle of the gastrocnemius. Hematoxylin and eosin staining were performed according to standard histology and histochemistry procedures (*58, 59*). Immunofluorescence was performed by first airdrying the sections for 30 minutes, followed by wetting the sections with PBS. Sections were then blocked (5% milk in PBS + 0.05% Tween 20 (PBST)) for an hour at room temperature (RT), followed by one hour incubation with primary antibodies indicated in Table S1. Muscle sections were then washed with PBST and incubated with secondary antibodies, including Dapi (2.5 µg/mL), for one hour. The sections were mounted using polymount after three PBST washes. Imaging over the whole cross sectional area was then performed using the CellInsight CX7 microscope (Thermo Fisher Scientific).

Cell culture and siRNA transfection

Immortalized human skeletal muscle cells (7304.1, (*60*)) were cultured in growth medium (F10 (Gibco) medium supplemented with 15% FCS, 1 ng/ml bFGF, 10 ng/ml EGF and 0.4 µg/ml Dexamethasone). Differentiation was induced using differentiation medium (DMEM (Gibco), without any supplements) for 24h to 72h. Muscle induced pluripotent stem cells (muscle progenitors (*61*)) were cultured in DMEM containing 10% FCS, 1% penicillin–streptomycin and 100 ng/mL bFGF (freshly added). Muscle progenitors were differentiated using DMEM containing 1% Insulin-Transferrin-Selenium-Ethanolamine (ITS-X) and 1% Knockout Serum Replacement (KOSR). siRNAs were transfected (Table S2) using Lipofectamine RNAiMAX transfection reagent, according to the manufacturer's manual (Thermo

Fisher Scientific). Cell cultures, at roughly 50% confluence, were transfected with 10 nM siRNA and grown for 48h in transfection medium (80% proliferation medium and 20% OptiMEM). Subsequently, medium was replaced either with normal proliferation or differentiation medium, or cells were directly harvested according to the experimental setup. Treatments with IFN were carried out with the human interferon IFN-α2 (PBL Assay Science, Cat. No. 11105-1) or recombinant Human IFN-β (Peprotech, Cat. No. 300-02BC) and were used at 1000 U/mL for 24h (unless indicated otherwise). Cell growth rate was determined with the phase contrast channel of the IncuCyte Zoom Imager (Essen Bioscience). An interval of 6h was used to determine the effect of USP18 knockdown on cell growth indicated by the percent confluence over time.

Muscle bundle assay

Muscle bundles were generated as described previously with small adjustments (*47, 62*). Muscle progenitor cells were used to create the bundles. Muscle progenitors were trypsinized, after which proliferation medium was added. Cells were subsequently centrifuged and trypsin-containing medium was aspirated. Next, muscle progenitors were diluted in cold growth medium without antibiotics. An ice-cold hydrogel, consisting of 20% Growth Factor Reduced Matrigel (Corning) and 2 mg/ml bovine fibrinogen (Sigma-Aldrich) was combined with muscle progenitors ($6x10^5$ cells per bundle). Knockdowns were induced by directly adding the USP18 (or siGenome) siRNA-lipofectamine particles at 200 nM to the muscle progenitor cells before adding this to the ice-cold hydrogel mix. Bovine Thrombin (0.8 units) (Sigma-Aldrich) was added to the hydrogel mix before casting the bundle in the polydimethylsiloxane (PDMS) chambers. After full polymerization (after casting 30 min at 37 °C), the newly formed bundles were kept in standard 2D muscle progenitor proliferation medium containing 1.5 mg/mL 6-aminocaproic acid (6-ACA) (Sigma-Aldrich). After 48 hours, proliferation medium was changed to differentiation medium (containing 2 mg/mL 6-ACA) and bundles were incubated on a platform shaker at 37 °C, 5% CO_2. Half of the differentiation medium was changed every other day. Twitch (1 Hz) and tetanic (20 Hz) contractions were measured after seven days of differentiation using an in-house setup. In brief, a cathode and anode were placed on either one of the PDMS pillars. An electrical pulse at 1 or 20 Hz was applied causing the muscle bundles to contract. Contractile force was calculated based on the displacement of the pillars of one contraction, which was recorded using live microscopy. The specific force was then calculated and normalised to cross sectional area of the muscle bundle. The bundles were subsequently either fixed overnight in 2% PFA for immunofluorescent staining and stored in PBS at 4 °C or frozen in liquid nitrogen and stored in -80 °C for RNA extraction.

Protein analyses

Western blot analyses
Proteins extracts were obtained using RIPA lysis buffer (20 mM Tris, pH 7.4, 150 mM NaCl, 5 mM EDTA, 1% NP40, 0.1% SDS and 1 mM DTT and 1x protease inhibitor cocktail). Next, 25 µg was separated on SDS-PAGE (Criterion XT, Bio-Rad). Proteins were then transferred to PVDF membranes, which after one hour blocking (5% milk in PBST) were blotted for the primary antibodies and subsequently with secondary antibodies (Table S1). An Odyssey CLx Infrared imaging system (LiCOR, NE. USA) was used to detect the fluorescent signal. Quantification of protein abundance was done using Image Studio Software version 5.2. Values were corrected for background and normalised to loading controls.

Mass spectrometry and analysis
7304.1 cell cultures were harvested by directly adding lysis buffer (20 mM HEPES (pH 8.0), 150 mM NaCl, 0.2% NP40, 10% glycerol and freshly added protease inhibitor cocktail (Roche)) to the cell culture dishes. 100 µg protein lysate was taken for in-solution digestion. First, samples were reduced using DTT (5 mM final concentration) for 30 min at 37 °C. Next, iodoacetamide was used to alkylate the samples (final concentration 20 mM, 15 min RT in the dark). Methanol/chloroform extraction method was then used to precipitate proteins, after which proteins were resuspended in 50 µL of 6 M urea and subsequently diluted to reduce urea concentration to <1M. Proteins were digested with trypsin (final concentration 0.2 µg/µL) on an overhead rotor at 12 rpm overnight. Digested peptides were subsequently acidified using trifluoroacetic acid (final concentration 1%) and desalted using C18 solid-phase extraction cartridges following the manufacturer's instructions (SEP-PAK plus, Waters). Reconstituted peptides (in 98% MilliQ, 2% CH_3CN and 0.1 %TFA) were analysed by nano-liquid chromatography tandem mass spectrometry (LC-MS/MS) using the Ultimate 3000 UHPLC (Thermo Fisher Scientific) connected to an Orbitrap Fusion Lumos Tribrid mass spectrometer (Thermo Fisher Scientific) using a one-hour gradient and universal settings for data acquisition as detailed previously (*63*).

Maxquant software (v1.6.10.43) was then used to search the raw MS files against the UniProtKB human sequence database (UP000005640, 79,038 human sequence entries). Next, the following parameters were set to perform label free quantification: Modification were set on Carbamidomethyl (C) as fixed and Oxidation (M) and Deamidation (NQ) as variable and a maximum of two missed cleavages were allowed. Match between runs function was not used. The quantified proteome was then analysed using Perseus (v.1.6.14.0), where significance was assessed using a student's t-test with multiple testing using permutation false discovery rate (FDR) set on 0.05 or 0.25 and s0 = 0.1, since the cultures were strongly heterogenic (less than half was fused).

Immunofluorescence staining
Cell cultures were fixed (10 min, 4% PFA), permeabilized (10 min at -20 °C with ice cold MeOH), blocked (1h, 5% BSA) and stained using antibodies against USP18, ISG15 and MyHC (Table S1). USP18 antibody was incubated overnight at 4 °C whereas all other antibodies were incubated for 1h at room temperature. Muscle bundles were stained for titin as previously described (*62*). Imaging of both 2D and 3D muscle models were carried out using the CellInsight CX7 microscope and a cell-based analysis was carried out using the accompanied HCS Platform software (Thermo Fisher Scientific). 3D muscle bundles were imaged with 20X objective using confocal for 40 stacks at 5 µm, images show maximum projections.

Calcium flux staining, imaging and analysis
Calcium flux analysis was carried out in 7304.1 cells 96h after transfection, allowing mature myotubes to form. Fluo-4 calcium imaging kit (Invitrogen) was then used according to the manufacturer's instructions. Neuro background suppressor was added 1:5 in 50 µL normal medium before imaging. Live cell imaging was carried out with the BZ-X800 Live-Cell Imaging Microscope (Keyence) using the 20X objective. The fluorescent signal was recorded for 30 seconds prior to KCl stimulation, which was done by directly adding 50 µL of normal medium containing 20 µM KCl to the well. Live cell imaging was stopped after circa 45 seconds of KCl stimulation. Analysis was performed using CALIMA (*64*). Average calcium fluxes were calculated over myoblasts or myotubes from 3 wells that were correctly segmented by CALIMA software.

Gene analyses

RNA was extracted using Qiazol, precipitated using chloroform followed by RNA isolation using the PureLink™ RNA Mini Kit (Invitrogen) according to the manual. cDNA synthesis was carried out with the RevertAid H Minus First Strand cDNA Synthesis Kit according to the user guide (Thermo Fisher Scientific). Quantitative RT-qPCR was performed using SYBR® Green Master mix (Bio-Rad). Samples were run in biological and technical triplicates using the LightCycler 480 System (Roche Diagnostics). The following primers were used to assess gene expression: *MEF2A* Fw 'TGAAAGCAGAACCAACTCGGA' and Rv 'GTAGGACAAAGCATTGGGGC'; *MYH3* Fw 'TCAAAGAGTTGCAGGCTCGAA' and Rv 'CATAGTCGCTGCGCTGTTTC'; *USP18* Fw 'CAACGTGCCCTTGTTTGTC' and Rv 'TGCAGTCTCTCCACCAAGTG';
MYH8 Fw 'ACATTACTGGCTGGCTGGAC' and Rv 'TTCGCGCTGCTATCTGCTTC';
MYOD Fw 'CGACGGCATGATGGACTACA' and Rv 'GCAGTCTAGGCTCGACACC';
MYOG Fw 'GCTCAGCTCCCTCAACCAG' and Rv 'GTGAGCAGATGATCCCCTGG';
and *TBP* as housekeeping gene with Fw 'CGCCGAATATAATCCCAAGCG' and Rv 'CCTGTGCACACCATTTTCCC'.

RNA sequencing and analysis

Poly(A) library preparation and sequencing were carried out by GENEWIZ Germany GmbH as follows. RNA samples were quantified using Qubit 4.0 Fluorometer (Life Technologies, Carlsbad, CA, USA) and RNA integrity was checked with RNA Kit on Agilent 5300 Fragment Analyzer (Agilent Technologies, Palo Alto, CA, USA). RNA sequencing libraries were prepared using the NEBNext Ultra II RNA Library Prep Kit for Illumina following the manufacturer's instructions (NEB, Ipswich, MA, USA). Briefly, mRNAs were first enriched with Oligo(dT) beads. Enriched mRNAs were fragmented for 15 minutes at 94 °C. First strand and second strand cDNAs were subsequently synthesized. cDNA fragments were end repaired and adenylated at 3'ends, and universal adapters were ligated to cDNA fragments, followed by index addition and library enrichment by limited-cycle PCR. Sequencing libraries were validated using NGS Kit on the Agilent 5300 Fragment Analyzer (Agilent Technologies, Palo Alto, CA, USA), and quantified by using Qubit 4.0 Fluorometer (Invitrogen, Carlsbad, CA). The sequencing libraries were multiplexed and loaded on the flowcell on the Illumina NovaSeq 6000 instrument according to manufacturer's instructions. The samples were sequenced using a 2x150 Pair-End (PE) configuration v1.5. Image analysis and base calling were conducted by the NovaSeq Control Software v1.7 on the NovaSeq instrument. Raw sequence data (.bcl files) generated from Illumina NovaSeq was converted into fastq files and de-multiplexed using Illumina bcl2fastq program version 2.20. One mismatch was allowed for index sequence identification.

RNA-Seq files were processed using the opensource BIOWDL RNAseq pipeline v5.0.0 (https://zenodo.org/record/5109461#.Ya2yLFPMJhE) developed at the LUMC. This pipeline performs FASTQ preprocessing (including quality control, quality trimming, and adapter clipping), RNA-Seq alignment, read quantification, and optionally transcript assembly. FastQC was used for checking raw read QC. Adapter clipping was performed using Cutadapt (v2.10) with default settings. RNA-Seq reads' alignment was performed using STAR (v2.7.5a) on GRCh38 human reference genome. The gene read quantification was performed using HTSeq-count (v0.12.4) with setting "–stranded=no". The gene annotation used for quantification was Ensembl version 104. Differentiation expression analysis was carried out with DESeq2 (*65*). P-values were corrected for multiple testing using Benjamini and Hochberg's.

General statistics and bioinformatics

Statistical significance for experiments in cell cultures was assessed using a student's T-test with N=3, unless depicted otherwise. Enrichment analyses were performed using DAVID bioinformatics resources v6.8 (https://david.ncifcrf.gov/) with the following settings: Medium confidence score, total proteome (N=3349) or total

transcriptome (N=11631) as background. Subsequent protein-protein interaction networks were analysed using STRING (https://string-db.org/; v11.5) and visualised with Cytoscape (v.3.8.2). Only significantly enriched clusters (Bonferroni FDR<0.05) of N>5 were considered.

Fig. 1

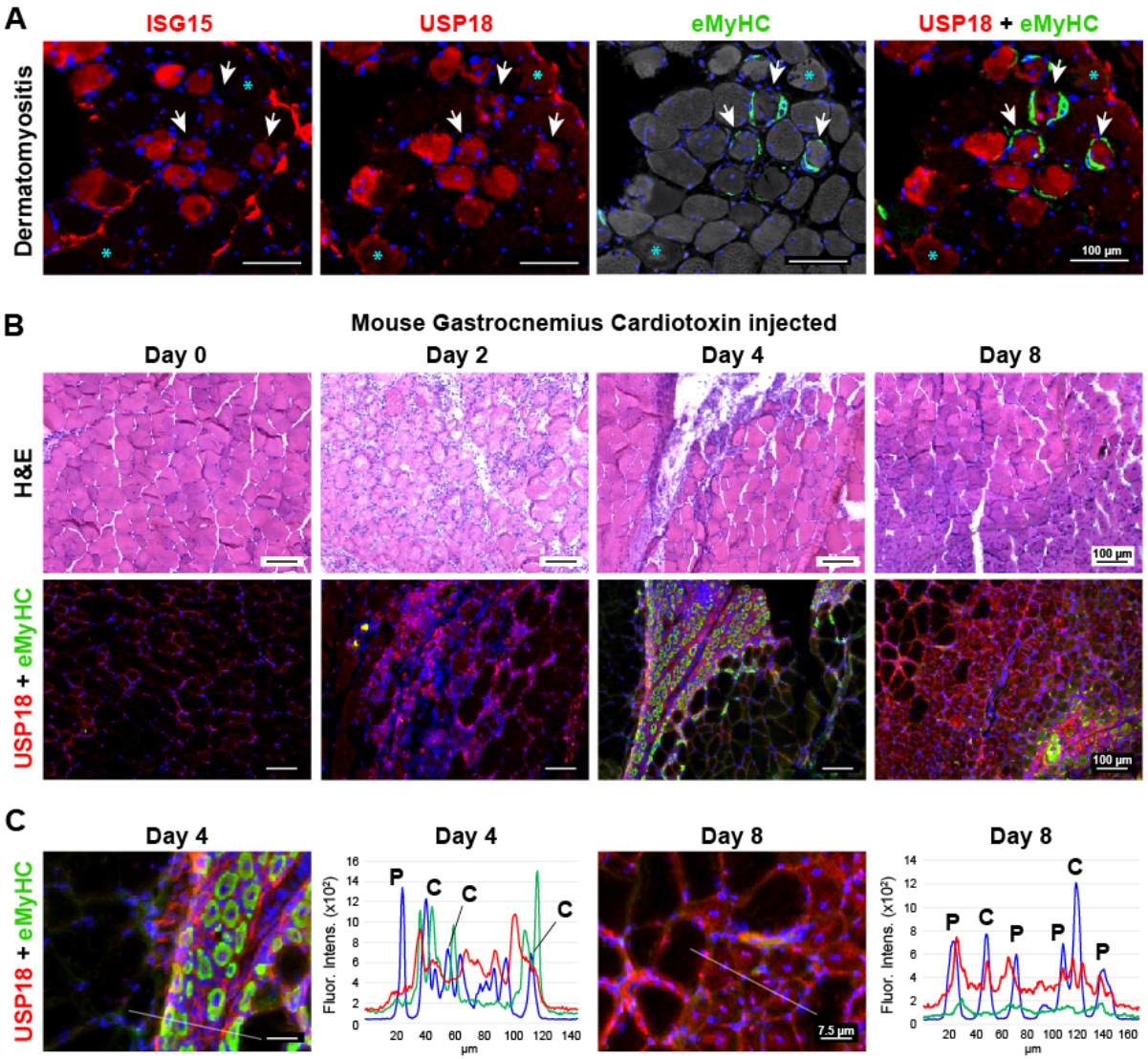

Figure 1. USP18 positive myofibers are at sites of regeneration. (**A**) Sequential muscle cross-sections of a dermatomyositis patient stained for ISG15, USP18, eMyHC; a merged image of USP18 and eMyHC is at the right panel. Examples of centrally nucleated myofibers positive for USP18 and surrounded by eMyHC positive cells are depicted by white arrows. Myofibers stained for USP18 but not for ISG15 are depicted by an cyan asterisk. Scale bars indicate 100 µm. (**B-C**) Mouse gastrocnemius muscles treated with cardiotoxin. (**B**) Muscle sections stained for H&E (upper panel), or for USP18 (red) and eMyHC (green) (lower panel) without (0) or after cardiotoxin injection (2, 4 or 8 days). Scale bar is 100 µm. (**C**) High magnifications of regions positive for USP18 at day 4 and 8. Scale bar is 7.5 µm. An overlap of fluorescent intensity distribution between DAPI (blue), USP18 (red) and eMyHC (green), corresponding to the white transparent line in the image, is plotted next to each image. Central nuclei are depicted with C, and peripheral nuclei with P. Nuclei are counter-stained with DAPI (blue).

Fig. 2

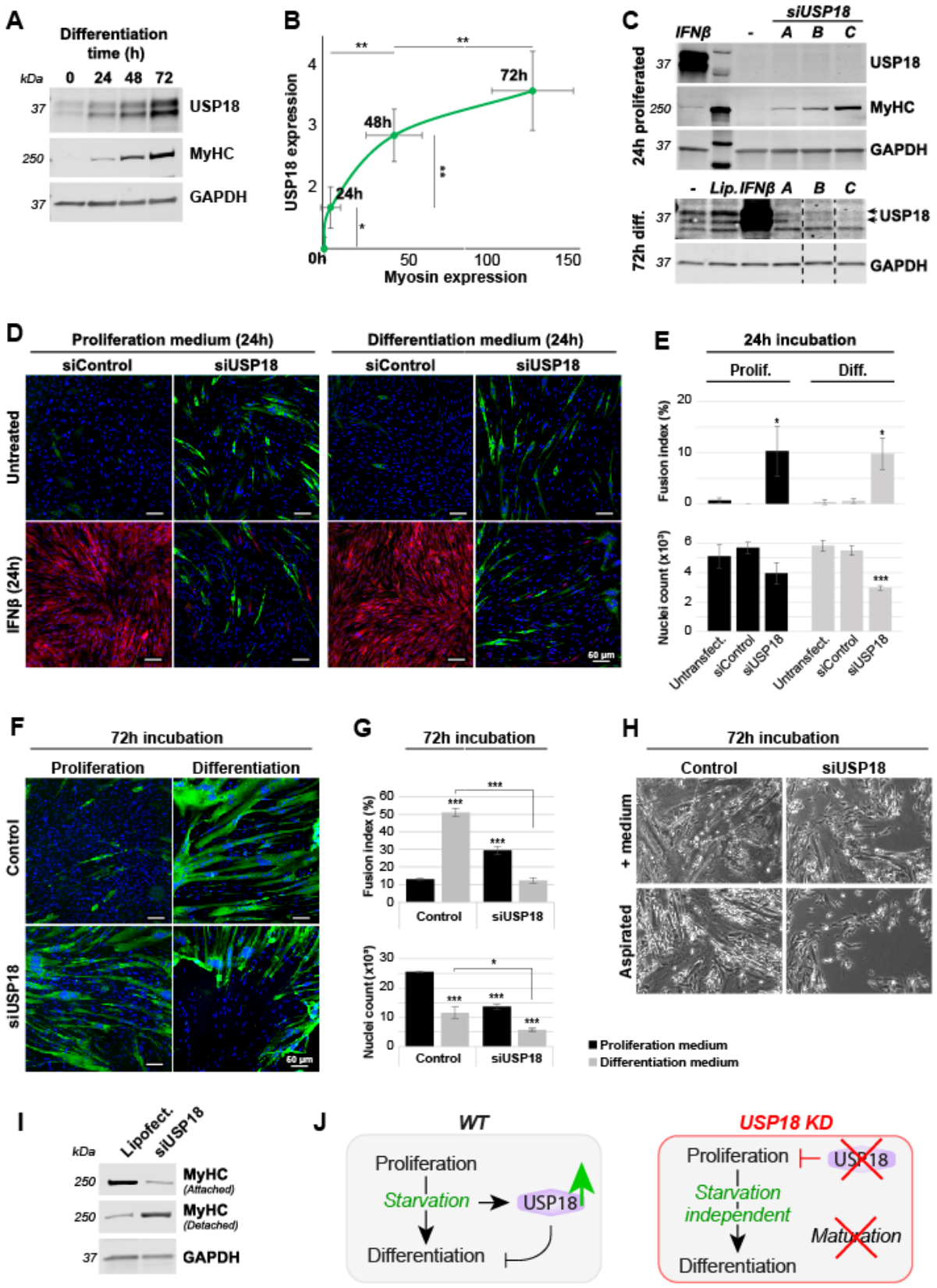
A
Differentiation time (h)
kDa 0 24 48 72
37 USP18
250 MyHC
37 GAPDH
B
USP18 expression
Myosin expression
0h
24h
48h
72h
C
siUSP18
IFNβ - A B C
24h proliferated
USP18
MyHC
GAPDH
- Lip. IFNβ A B C
72h diff.
USP18
GAPDH
D
Proliferation medium (24h)
Differentiation medium (24h)
siControl
siUSP18
Untreated
IFNβ (24h)
50 µm
E
24h incubation
Prolif.
Diff.
Fusion index (%)
Nuclei count (x10³)
Untransfect.
siControl
siUSP18
F
72h incubation
Proliferation
Differentiation
Control
siUSP18
50 µm
G
72h incubation
Fusion index (%)
Nuclei count (x10³)
Control
siUSP18
H
72h incubation
Control
siUSP18
+ medium
Aspirated
Proliferation medium
Differentiation medium
I
Lipofect.
siUSP18
kDa
250 MyHC (Attached)
250 MyHC (Detached)
37 GAPDH
J
WT
Proliferation
Starvation
USP18
Differentiation
USP18 KD
Proliferation
USP18
Starvation independent
Maturation
Differentiation

Figure 2. USP18 knockdown (KD) induces differentiation reprograming. (**A**) A representative western blot shows USP18 expression during muscle cell differentiation marked by MyHC. GAPDH was used as loading control. (**B**) Scatter plot shows USP18 levels against MyHC levels normalised to GAPDH at 0h, 24h, 48h and 72h of differentiation. Average and error bars (standard deviation (SD)) are from four biological replicates. (**C**) Western blots show USP18 levels after incubation in proliferating or differentiating medium. MyHC marks increased differentiation in proliferation medium. GAPDH was used as loading control. In proliferating cell cultures, USP18 is under the detection level. IFNβ treatment was used as positive control for USP18 expression. (**D**) Representative immunofluorescence images show MyHC (green) and USP18 (red) in USP18 KD cells cultured in proliferation or differentiation medium. A USP18 KD is demonstrated in cultures treated with IFNβ. Nuclei are coloured in blue. Scale bar is 50 μm. (**E**) Bar charts show fusion index and cell number in USP18 KD cell cultures in proliferation (Prolif.) or differentiation (Diff.) medium (in black or grey bars, respectively). Average and error bars (SD) are from 3 replicates. (**F**) Representative immunofluorescence images of control or USP18 KD cells cultured in proliferation or differentiation medium for 72 hours. Myotubes are marked with MyHC (green), and nuclei (blue) mark cell density. (**G**) Bar charts show the fusion index and the nuclear count for the four conditions as in panel F. Average and error bars (SD) are from N=3 biological replicates. Statistical significance is depicted by asterisks. (*: 0.05-0.005, **: 0.005-0.0005, *** <0.0005). (**H**) Images taken with a brightfield microscopy show the cultures before collection for protein extraction. (**I**) A western blot shows MyHC levels in attached cells after 72h incubation and in the medium collected from the same cultures (=detached) of muscle progenitors after USP18 KD. GAPDH of attached cells is used as loading control. (**J**) A graphical working model of USP18 effect on muscle cell differentiation. WT: normal conditions (left panel); in the absence of USP18 KD (right panel), differentiation is starvation independent.

Fig. 3

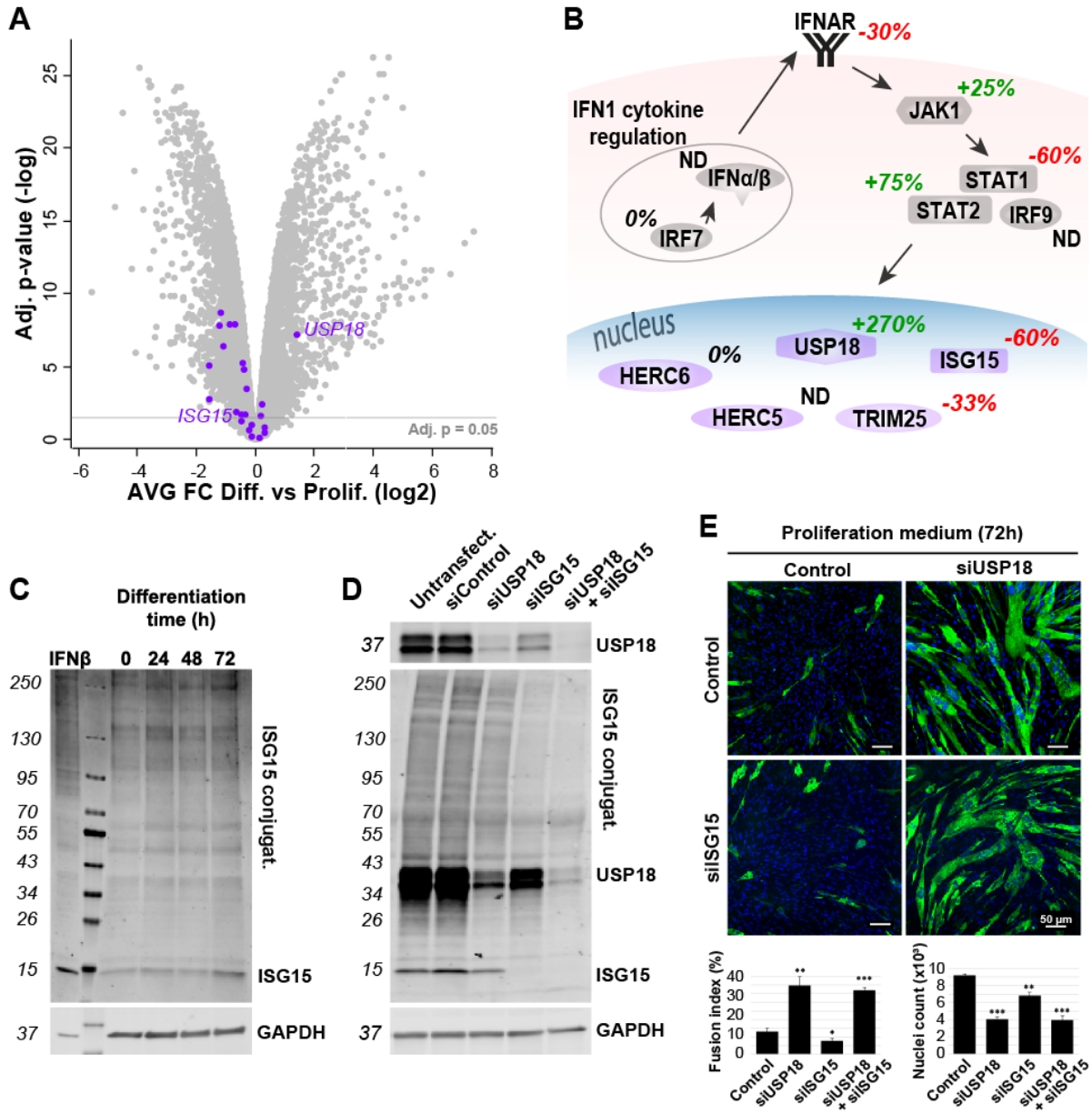

Figure 3. Elevated USP18 expression during muscle cell differentiation is IFN-1-independent. (**A**) Volcano plot shows mRNA fold change vs. p-value between proliferation and differentiating cultures. The interferon type-1 induced genes are highlighted in purple. The adjusted p-value of 0.05 is depicted. (**B**) A schematic presentation of the canonical IFN-1 pathway. The fold change of genes whose expression profile is significantly changed during muscle cell differentiation is depicted in green (upregulated) or red (downregulated); ND = not detected; non-significant = 0%. The IFN-1 stimulated genes are coloured in purple and genes in the IFN-1 signalling cascade are coloured in grey. (**C**) Western blot against ISG15 during muscle cell differentiation. GAPDH is used as loading control and IFNβ treatment was used as positive control. (**D**) Western blots show USP18, ISG15 and ISG15

conjugates in siUSP18, siISG15 or siUSP18 + siISG15 double KD cell cultures treated with IFNβ treatment (1000U/mL) for 24h in proliferating medium. GAPDH was used as loading control. (**E**) Representative immunofluorescence images show MyHC staining in siUSP18, siISG15 or siUSP18 + siISG15 cell cultures incubated in proliferation medium for 72h. Nuclei are counter-stained with DAPI (blue). Scale bar is 50 µm. Bar charts show fusion index for the respective cell cultures. Average and error bars (SD) are from N=3. Statistical significance is depicted with asterisks. (*: 0.05-0.005, **: 0.005-0.0005, *** <0.0005).

Fig. 4

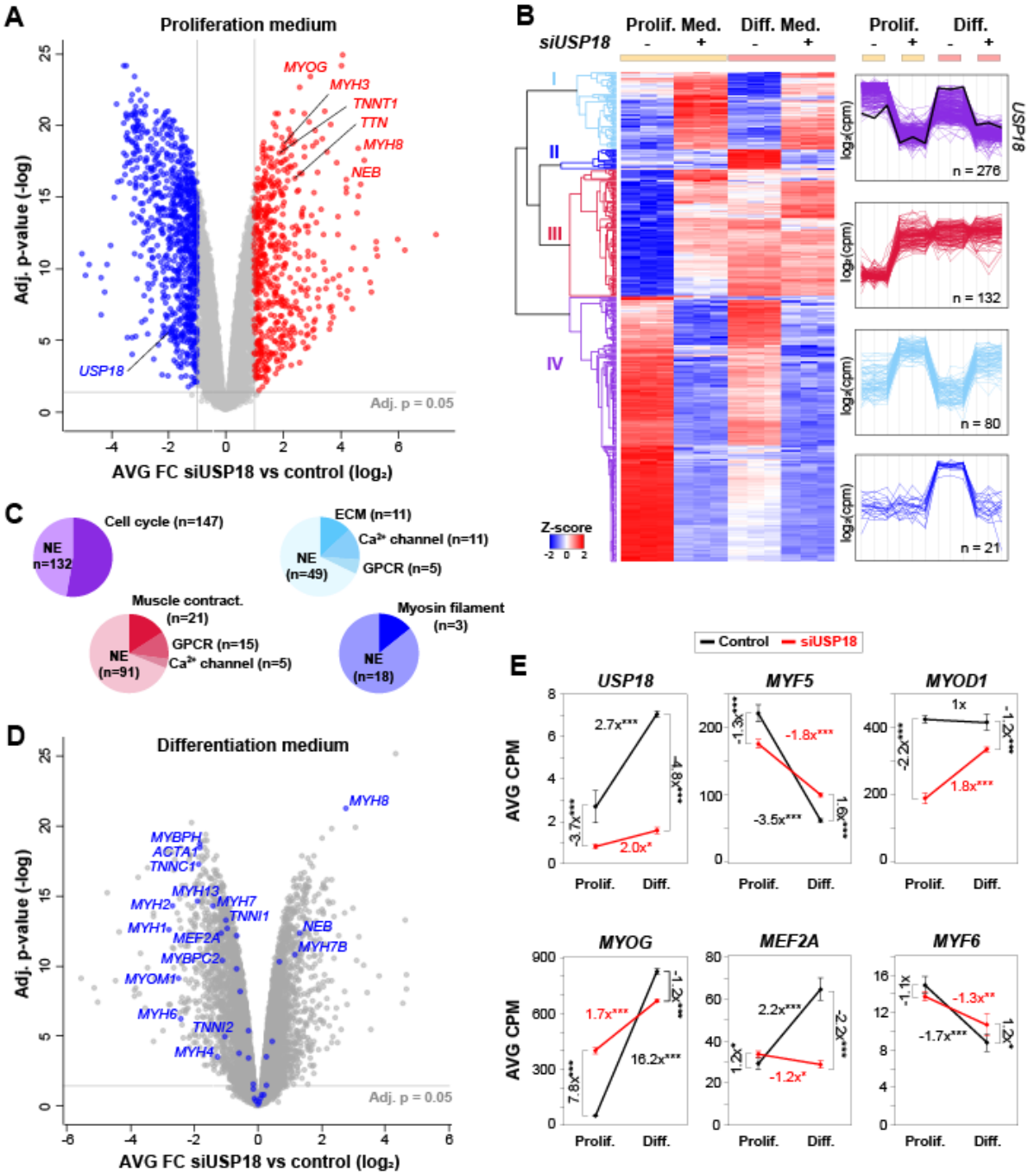
A
Proliferation medium
Adj. p-value (-log)
AVG FC siUSP18 vs control (log₂)
MYOG
MYH3
TNNT1
TTN
MYH8
NEB
USP18
Adj. p = 0.05
B
siUSP18
Prolif. Med.
Diff. Med.
Prolif.
Diff.
I
II
III
IV
Z-score
n = 276
n = 132
n = 80
n = 21
C
Cell cycle (n=147)
NE n=132
ECM (n=11)
Ca²⁺ channel (n=11)
GPCR (n=5)
NE (n=49)
Muscle contract. (n=21)
GPCR (n=15)
Ca²⁺ channel (n=5)
NE (n=91)
Myosin filament (n=3)
NE (n=18)
D
Differentiation medium
MYH8
MYBPH
ACTA1
TNNC1
MYH13
MYH2
MYH7
TNNI1
MYH1
MEF2A
NEB
MYH7B
MYBPC2
MYOM1
MYH6
TNNI2
MYH4
Adj. p = 0.05
E
Control
siUSP18
USP18
MYF5
MYOD1
MYOG
MEF2A
MYF6
AVG CPM
Prolif.
Diff.
F
Muscle specific regulators
Proliferating
- MYF5
- MYOD1
Differentiating
- MEF2
- MYOG
Control
Proliferation
Starvation
MYF5
MYOD1
MEF2A
MYOG
Proliferating
Differentiated
USP18 KD
Proliferation
Starvation
MYF5
MYOD1
MEF2A
MYOG
Differentiated

Figure 4. USP18 KD leads to reduced expression of cell cycle genes and re-programming of myogenic regulatory factors. (**A**) Volcano plot shows mRNA average fold changes in USP18 KD cells cultured in proliferating medium (N=3). A fold change (FC) cut off (>|2|) and the statistical significance ($p<0.05$, FDR) are indicated. Genes surpassing these thresholds are depicted in blue (FC<-2) or red (FC> 2). (**B**) Heatmap shows hierarchical clustering of the most affected genes that surpassed the selection criteria (FC>|4|, Adj. p-value<0.05) of the following comparisons: Control vs. siUSP18 cultured in proliferating or differentiating medium. Adjacent plots show expression profiles of the four largest clusters depicted in cyan (I) blue (II), red (III) or purple (IV). USP18 expression profile is marked with a black line. (**C**) Pie charts show the enriched gene networks per cluster. (**D**) Volcano plot shows mRNA average fold change of USP18 KD cultured in differentiation medium. Myogenic genes are highlighted in blue. (**E**) Dot plots show the average CPM for five myogenic regulatory genes in control (black) and USP18 KD (red) cells cultured in proliferation or differentiation medium. Average and error bars (SD) are from N=3. Statistical significance is depicted by asterisks. (*: 0.05-0.005, **: 0.005-0.0005, *** <0.0005). (**F**) Schematic overview shows the relative abundance of muscle-specific regulatory genes at 24 hours starvation or proliferation in control and USP18 KD cultures. Genes depicted in black show similar change direction in USP18 KD and control and depicted in red are genes whose expression direction is altered in USP18 KD cell culture.

Fig. 5

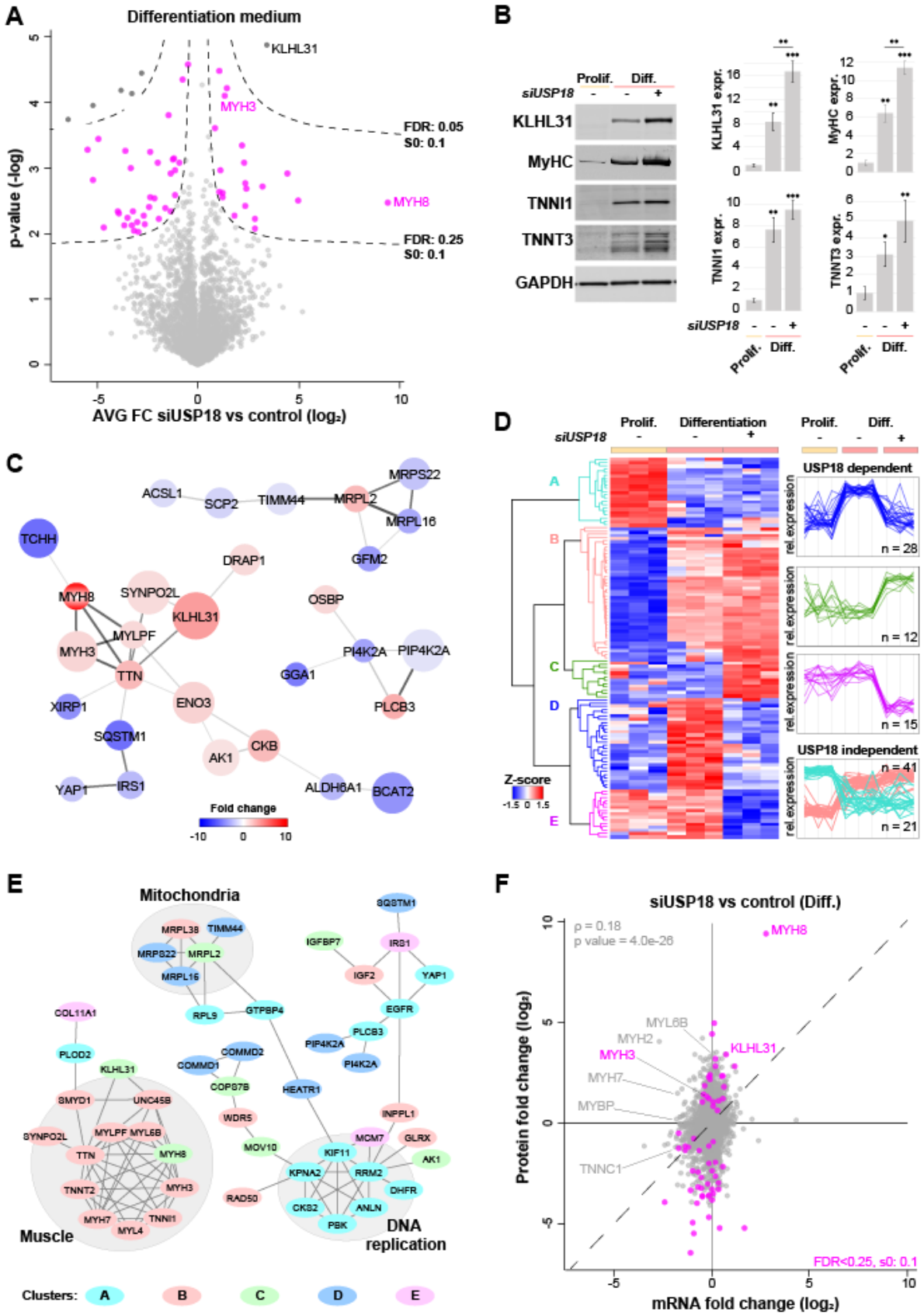
A
Differentiation medium
KLHL31
MYH3
MYH8
FDR: 0.05
S0: 0.1
FDR: 0.25
S0: 0.1
p-value (-log)
AVG FC siUSP18 vs control (log₂)
B
Prolif.
Diff.
siUSP18
KLHL31
MyHC
TNNI1
TNNT3
GAPDH
KLHL31 expr.
MyHC expr.
TNNI1 expr.
TNNT3 expr.
C
ACSL1
SCP2
TIMM44
MRPL2
MRPS22
MRPL16
TCHH
DRAP1
GFM2
MYH8
SYNPO2L
KLHL31
OSBP
MYLPF
MYH3
PI4K2A
PIP4K2A
TTN
GGA1
XIRP1
ENO3
PLCB3
SQSTM1
CKB
AK1
YAP1
IRS1
ALDH6A1
BCAT2
Fold change
D
Prolif.
Differentiation
Diff.
siUSP18
USP18 dependent
USP18 independent
rel. expression
n = 28
n = 12
n = 15
n = 41
n = 21
Z-score
E
Mitochondria
Muscle
DNA replication
Clusters:
F
siUSP18 vs control (Diff.)
ρ = 0.18
p value = 4.0e-26
MYH8
MYL6B
MYH2
MYH3
KLHL31
MYH7
MYBP
TNNC1
FDR<0.25, s0: 0.1
Protein fold change (log₂)
mRNA fold change (log₂)

Figure 5. USP18-dependent proteome shows higher expression levels of muscle proteins. (**A**) Volcano plot shows the protein average fold changes of USP18 KD cells cultured in differentiation medium (Diff.) (N=3). Sigmoid curves for FDR 0.05 and 0.25 are depicted by dashed lines. Proteins surpassing the 0.25 FDR threshold are highlighted in pink and in black FDR<0.05. (**B**) Representative western blots show the expression of four muscle-specific proteins. Bar charts show the quantifications for which GAPDH was used as loading control. Expression levels were normalised to control samples in proliferation condition. Average and error bars (SD) are from N=3 biological replicates. Statistical significance is depicted by asterisks. (*: 0.05-0.005, **: 0.005-0.0005, *** <0.0005). (**C**) Protein-protein interaction networks of the proteins that surpassed the FDR<0.25. Colour grade highlights the average fold change, and the larger the circle, the more significant (0.01->0.00001). The protein-protein interaction strength is highlighted by the thickness of the edges. (**D**) Heatmap shows hierarchical clustering for the significantly affected proteins (N=117) of the following comparisons: control vs. siUSP18 cultured in differentiation medium (N=63) and differentiation vs. proliferation medium (N=54). The protein expression profiles of the USP18-dependent clusters are coloured in blue, green, or magenta. The cyan and pink clusters represent the USP18-independent changes. (**E**) Protein-protein interaction networks of all 117 proteins, per protein the expression profile cluster is denoted in the corresponding colour. Protein networks are marked by grey circles. (**F**) Scatterplot shows the mRNA against protein fold change of USP18 KD cells cultured in differentiation medium. Proteins highlighted in pink pass the FDR<0.25, in grey are the non-significant proteins. Muscle proteins are highlighted. The dashed line indicates the diagonal, and the Spearman correlation is depicted in light grey.

Fig. 6

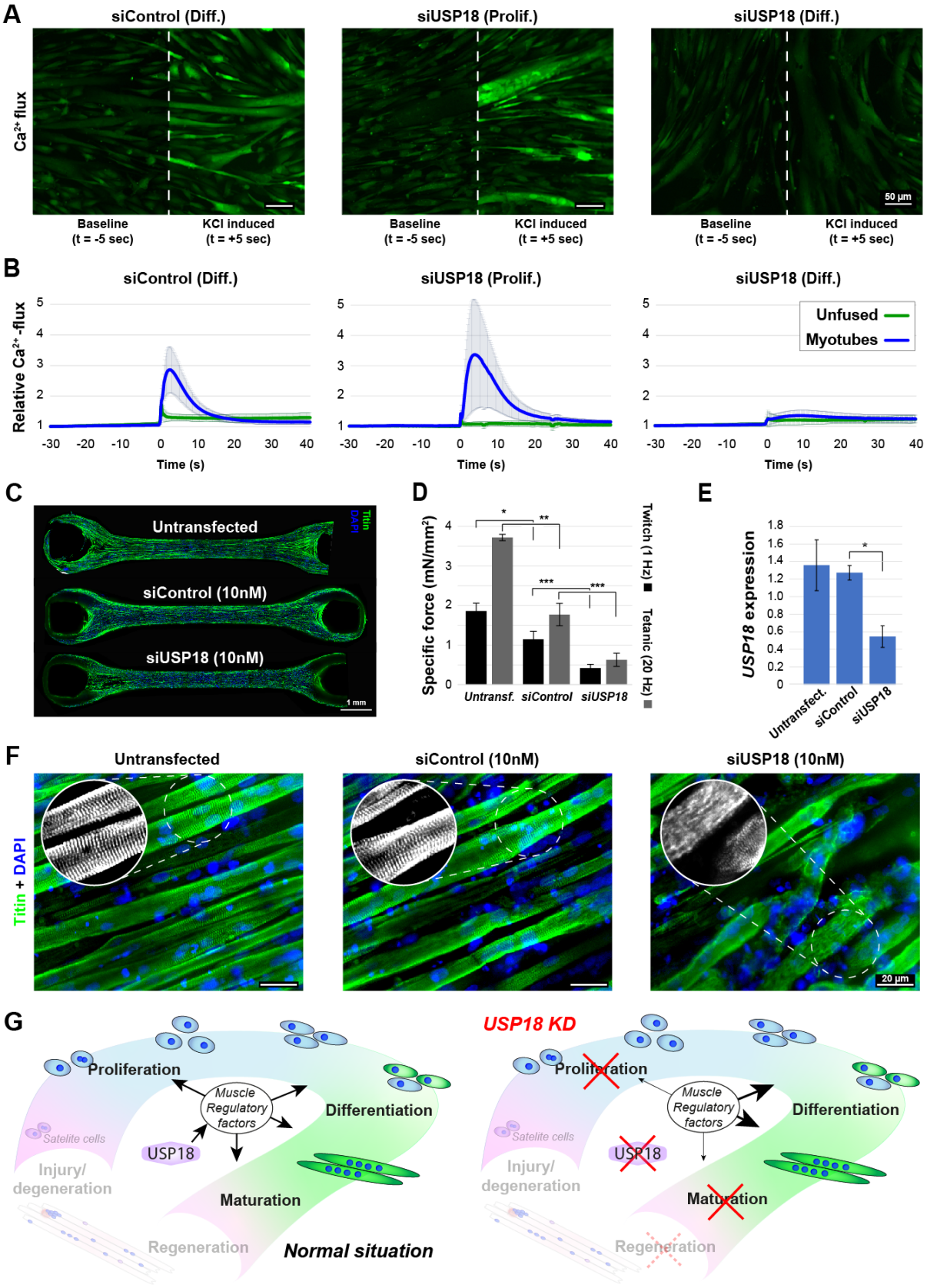
A
siControl (Diff.)
siUSP18 (Prolif.)
siUSP18 (Diff.)
Ca2+ flux
Baseline (t = -5 sec)
KCl induced (t = +5 sec)
50 µm
B
Relative Ca2+-flux
Time (s)
Unfused
Myotubes
C
Untransfected
siControl (10nM)
siUSP18 (10nM)
Titin
DAPI
1 mm
D
Specific force (mN/mm²)
Untransf.
siControl
siUSP18
Twitch (1 Hz)
Tetanic (20 Hz)
E
USP18 expression
Untransfect.
siControl
siUSP18
F
Untransfected
siControl (10nM)
siUSP18 (10nM)
Titin + DAPI
20 µm
G
Proliferation
Muscle Regulatory factors
Differentiation
Satelite cells
USP18
Injury/ degeneration
Maturation
Regeneration
Normal situation
USP18 KD

Figure 6. USP18 KD negatively affects *in vitro* muscle physiology. (**A**) Representative images of the calcium flux (green signal) 5 seconds before or after KCl (10 mM) administration in cells transfected with siControl in differentiation medium (Diff.) or with siUSP18 in proliferation or differentiation medium. The respective images are separated by a white dashed line. Scale bar is 50 µm. (**B**) Graphs show changes in calcium flux over time. Calcium flux in uni-nucleated cells (unfused) is depicted by a green line and multi-nucleated cells (myotubes) by a blue line. Average and error bars (SD) are from N=3 biological replicates. (**C**) An image of a representative bundle stained for titin (green) and nuclei (blue) for each genetic condition. Scale bar is 1 mm. (**D**) Bar chart shows the specific contractile forces (in mN/mm^2) at 7 days of differentiation for USP18 KD and controls. Twitch (1 Hz) and tetanic (20 Hz) contractions are depicted by black or grey bars, respectively. Average and SD are from contractions of four different muscle bundles. (**E**) Bar chart shows *USP18* expression levels normalised to untreated muscle bundles at 7 days of differentiation. Averages and SD are from N=3. Statistical significance in panel D and E is depicted by asterisks. (*: 0.05-0.005, **: 0.005-0.0005, *** <0.0005). (**F**) Representative images show the myofiber integrity after 7 days of differentiation. The coloured images show titin in green and nuclei in blue. Grey scale images show titin staining. Scale bar is 20 µm. (**G**) A model of muscle cell differentiation in presence or absence of USP18. During normal muscle cell differentiation, USP18 regulates multiple steps, including proliferation, differentiation and maturation. In absence of USP18, cell proliferation is inhibited accelerating differentiation, whereas maturation is not maintained.

Acknowledgements
We would like to thank Maaike van Putten for kindly providing the CTX injected mice muscles. We would also like to thank the TDI MS Laboratory/Discovery Proteomics Facility for their technical support.

Funding: This study was funded by grants from the Chinese Academy of Medical Sciences (CAMS) Innovation Fund for Medical Science (CIFMS), China (grant number: 2018-I2M-2-002) (B.M.K, A.P.F.), Pfizer (B.M.K, A.P.F) and the Engineering and Physical Sciences Research Council (EP/N034295/1) to (B.M.K), AFM 26110 to VR, and funding from the Department of Human Genetics to VR. Authors of this publication are members of the Netherlands Neuromuscular Center (NL-NMD) and the European Reference Network for rare neuromuscular diseases EURO-NMD.

Author contributions: C.S.O., V.R. and B.M.K. directed this study. C.S.O. conducted most experiments and analyses. A.P.F. helped with mass spectrometry sample preparation and data interpretation. A.D. helped with cell culture experiment. S.A. performed H&E staining and subsequent imaging. H.M. analysed the RNAseq. B.H. performed gene expression analysis for muscle bundles. E.W. and J.G. helped with muscle bundle culture and contractile analysis. A.J.K., J.R. and E.A. collected and provided human muscle biopsies. I.V. performed mass spectrometry. Manuscript was written by C.S.O, B.M.K and V.R.; All authors commented on the manuscript.

Competing interests: All authors declare no conflict of interest.

Data availability: The mass spectrometry data set has been deposited to the ProteomeXchange Consortium (http://proteomecentral.proteomexchange.org) via the PRIDE partner repository (*66*) and is available through the dataset identifier PXD032406. The transcriptomics dataset is deposited in NCBI's Gene Expression Omnibus (GEO) (*67*) and is accessible under the accession number GSE198794, https://www.ncbi.nlm.nih.gov/geo/query/acc.cgi?acc=GSE198794.

References

1. I. E. Lundberg *et al.*, Idiopathic inflammatory myopathies. *Nature Reviews Disease Primers* **7**, 86 (2021).
2. L. Bolko *et al.*, The role of interferons type I, II and III in myositis: A review. *Brain Pathology* **31**, e12955 (2021).
3. S. A. Greenberg, Dermatomyositis and type 1 interferons. *Current rheumatology reports* **12**, 198-203 (2010).
4. C. Hou *et al.*, From Diagnosis to Prognosis: Revisiting the Meaning of Muscle ISG15 Overexpression in Juvenile Inflammatory Myopathies. *Arthritis & rheumatology (Hoboken, N.J.)* **73**, 1044-1052 (2021).
5. G. A. Cobos, A. Femia, R. A. Vleugels, Dermatomyositis: An Update on Diagnosis and Treatment. *American Journal of Clinical Dermatology* **21**, 339-353 (2020).
6. F. McNab, K. Mayer-Barber, A. Sher, A. Wack, A. O'Garra, Type I interferons in infectious disease. *Nature Reviews Immunology* **15**, 87-103 (2015).
7. J. Qian, H. Xu, COVID-19 Disease and Dermatomyositis: A Mini-Review. *Frontiers in immunology* **12**, 747116 (2021).
8. R. Peravali, S. Acharya, S. H. Raza, D. Pattanaik, M. B. Randall, Dermatomyositis Developed After Exposure to Epstein-Barr Virus Infection and Antibiotics Use. *The American journal of the medical sciences* **360**, 402-405 (2020).
9. C. Villarroya-Beltri, S. Guerra, F. Sánchez-Madrid, ISGylation - a key to lock the cell gates for preventing the spread of threats. *Journal of cell science* **130**, 2961-2969 (2017).
10. L. A. Durfee, N. Lyon, K. Seo, J. M. Huibregtse, The ISG15 conjugation system broadly targets newly synthesized proteins: implications for the antiviral function of ISG15. *Molecular cell* **38**, 722-732 (2010).
11. J. M. Park *et al.*, Modification of PCNA by ISG15 plays a crucial role in termination of error-prone translesion DNA synthesis. *Molecular cell* **54**, 626-638 (2014).
12. A. Pinto-Fernandez *et al.*, Deletion of the deISGylating enzyme USP18 enhances tumour cell antigenicity and radiosensitivity. *Br J Cancer* **124**, 817-830 (2021).
13. T. Held, M. Basler, K. P. Knobeloch, M. Groettrup, Evidence for an involvement of the ubiquitin-like modifier ISG15 in MHC class I antigen presentation. *European journal of immunology* **51**, 138-150 (2021).
14. D. Munnur *et al.*, Altered ISGylation drives aberrant macrophage-dependent immune responses during SARS-CoV-2 infection. *Nature immunology* **22**, 1416-1427 (2021).
15. L. Ketscher *et al.*, Selective inactivation of USP18 isopeptidase activity in vivo enhances ISG15 conjugation and viral resistance. *Proceedings of the National Academy of Sciences of the United States of America* **112**, 1577-1582 (2015).
16. A. Basters *et al.*, Structural basis of the specificity of USP18 toward ISG15. *Nature structural & molecular biology* **24**, 270-278 (2017).
17. K.-i. Arimoto *et al.*, STAT2 is an essential adaptor in USP18-mediated suppression of type I interferon signaling. *Nature structural & molecular biology* **24**, 279-289 (2017).
18. F. Alsohime *et al.*, JAK Inhibitor Therapy in a Child with Inherited USP18 Deficiency. *New England Journal of Medicine* **382**, 256-265 (2020).
19. M. E. Meuwissen *et al.*, Human USP18 deficiency underlies type 1 interferonopathy leading to severe pseudo-TORCH syndrome. *The Journal of experimental medicine* **213**, 1163-1174 (2016).
20. T. Goldmann *et al.*, USP18 lack in microglia causes destructive interferonopathy of the mouse brain. *The EMBO Journal* **34**, 1612-1629 (2015).
21. W. Diao *et al.*, USP18 promotes cell proliferation and suppressed apoptosis in cervical cancer cells via activating AKT signaling pathway. *BMC cancer* **20**, 741 (2020).

22. L. Feng *et al.*, Deubiquitinase USP18 promotes the progression of pancreatic cancer via enhancing the Notch1-c-Myc axis. *Aging* **12**, 19273-19292 (2020).
23. J. A. Kang, Y. J. Jeon, Emerging Roles of USP18: From Biology to Pathophysiology. *Int J Mol Sci* **21**, 6825 (2020).
24. M. Salajegheh *et al.*, Interferon-stimulated gene 15 (ISG15) conjugates proteins in dermatomyositis muscle with perifascicular atrophy. *Annals of neurology* **67**, 53-63 (2010).
25. M. Agarwal *et al.*, Myosin heavy chain-embryonic regulates skeletal muscle differentiation during mammalian development. *Development (Cambridge, England)* **147**, (2020).
26. C. F. Bentzinger, Y. X. Wang, M. A. Rudnicki, Building muscle: molecular regulation of myogenesis. *Cold Spring Harb Perspect Biol*. 2012 (10.1101/cshperspect.a008342).
27. R. S. Krauss *et al.*, Close encounters: regulation of vertebrate skeletal myogenesis by cell-cell contact. *Journal of cell science* **118**, 2355-2362 (2005).
28. J. Cai *et al.*, Downregulation of USP18 inhibits growth and induces apoptosis in hepatitis B virus-related hepatocellular carcinoma cells by suppressing BCL2L1. *Experimental cell research* **358**, 315-322 (2017).
29. C. Multhauf, J. Lough, Interferon-mediated inhibition of differentiation in a murine myoblast cell line. *Journal of cellular physiology* **126**, 211-215 (1986).
30. S. Franzi, M. Salajegheh, R. Nazareno, S. A. Greenberg, Type 1 interferons inhibit myotube formation independently of upregulation of interferon-stimulated gene 15. *PloS one* **8**, e65362 (2013).
31. M. Rizzo *et al.*, Activation of the interferon type I response rather than autophagy contributes to myogenesis inhibition in congenital DM1 myoblasts. *Cell Death & Disease* **9**, 1071 (2018).
32. D. Jiménez Fernández, S. Hess, K.-P. Knobeloch, Strategies to Target ISG15 and USP18 Toward Therapeutic Applications. *Frontiers in Chemistry* **7**, (2020).
33. F. Vuillier, Z. Li, P.-H. Commere, L. T. Dynesen, S. Pellegrini, USP18 and ISG15 coordinately impact on SKP2 and cell cycle progression. *Scientific Reports* **9**, 4066 (2019).
34. N. L. Estrella *et al.*, MEF2 Transcription Factors Regulate Distinct Gene Programs in Mammalian Skeletal Muscle Differentiation*. *Journal of Biological Chemistry* **290**, 1256-1268 (2015).
35. P. S. Zammit, Function of the myogenic regulatory factors Myf5, MyoD, Myogenin and MRF4 in skeletal muscle, satellite cells and regenerative myogenesis. *Seminars in cell & developmental biology* **72**, 19-32 (2017).
36. M. Schmidt, S. C. Schüler, S. S. Hüttner, B. von Eyss, J. von Maltzahn, Adult stem cells at work: regenerating skeletal muscle. *Cellular and molecular life sciences : CMLS* **76**, 2559-2570 (2019).
37. H. Sasaki, H. Kohsaka, Current diagnosis and treatment of polymyositis and dermatomyositis. *Modern rheumatology* **28**, 913-921 (2018).
38. T. Le Voyer *et al.*, JAK inhibitors are effective in a subset of patients with juvenile dermatomyositis: a monocentric retrospective study. *Rheumatology* **60**, 5801-5808 (2021).
39. F. Chinyengetere *et al.*, Mice null for the deubiquitinase USP18 spontaneously develop leiomyosarcomas. *BMC cancer* **15**, 886 (2015).
40. L. A. Rempel *et al.*, Ubp43 gene expression is required for normal Isg15 expression and fetal development. *Reproductive biology and endocrinology : RB&E* **5**, 13 (2007).
41. K. J. Ritchie *et al.*, Dysregulation of protein modification by ISG15 results in brain cell injury. *Genes & development* **16**, 2207-2212 (2002).

42. Y. Guo *et al.*, Blockade of the ubiquitin protease UBP43 destabilizes transcription factor PML/RARα and inhibits the growth of acute promyelocytic leukemia. *Cancer Res* **70**, 9875-9885 (2010).
43. Y. Guo *et al.*, Evidence for the ubiquitin protease UBP43 as an antineoplastic target. *Molecular cancer therapeutics* **11**, 1968-1977 (2012).
44. J.-B. Fan *et al.*, Identification and characterization of a novel ISG15-ubiquitin mixed chain and its role in regulating protein homeostasis. *Scientific Reports* **5**, 12704 (2015).
45. K. P. Knobeloch, O. Utermöhlen, A. Kisser, M. Prinz, I. Horak, Reexamination of the role of ubiquitin-like modifier ISG15 in the phenotype of UBP43-deficient mice. *Molecular and cellular biology* **25**, 11030-11034 (2005).
46. J. W. Sanger *et al.*, in *The Actin Cytoskeleton,* B. M. Jockusch, Ed. (Springer International Publishing, Cham, 2017), pp. 39-75.
47. C. S. Olie *et al.*, Cytoskeletal disorganization underlies PABPN1-mediated myogenic disability. *Scientific Reports* **10**, 17621 (2020).
48. S. Lange, N. Pinotsis, I. Agarkova, E. Ehler, The M-band: The underestimated part of the sarcomere. *Biochimica et biophysica acta. Molecular cell research* **1867**, 118440 (2020).
49. C. Hang *et al.*, Knockout of MYOM1 in human cardiomyocytes leads to myocardial atrophy via impairing calcium homeostasis. *Journal of cellular and molecular medicine* **25**, 1661-1676 (2021).
50. A. Kalsotra *et al.*, The Mef2 transcription network is disrupted in myotonic dystrophy heart tissue, dramatically altering miRNA and mRNA expression. *Cell reports* **6**, 336-345 (2014).
51. C. A. Desjardins, F. J. Naya, Antagonistic regulation of cell-cycle and differentiation gene programs in neonatal cardiomyocytes by homologous MEF2 transcription factors. *The Journal of biological chemistry* **292**, 10613-10629 (2017).
52. L. Sun *et al.*, JAK1-STAT1-STAT3, a key pathway promoting proliferation and preventing premature differentiation of myoblasts. *J Cell Biol* **179**, 129-138 (2007).
53. W. Yang, P. Hu, Skeletal muscle regeneration is modulated by inflammation. *J Orthop Translat* **13**, 25-32 (2018).
54. L. Forcina, M. Cosentino, A. Musarò, Mechanisms Regulating Muscle Regeneration: Insights into the Interrelated and Time-Dependent Phases of Tissue Healing. *Cells* **9**, 1297 (2020).
55. B. Chazaud, Inflammation and Skeletal Muscle Regeneration: Leave It to the Macrophages! *Trends in immunology* **41**, 481-492 (2020).
56. M. Juhas *et al.*, Incorporation of macrophages into engineered skeletal muscle enables enhanced muscle regeneration. *Nature Biomedical Engineering* **2**, 942-954 (2018).
57. A. L. Mammen, Y. Allenbach, W. Stenzel, O. Benveniste, 239th ENMC International Workshop: Classification of dermatomyositis, Amsterdam, the Netherlands, 14-16 December 2018. *Neuromuscular disorders : NMD* **30**, 70-92 (2020).
58. L. R. Wedderburn *et al.*, International consensus on a proposed score system for muscle biopsy evaluation in patients with juvenile dermatomyositis: a tool for potential use in clinical trials. *Arthritis and rheumatism* **57**, 1192-1201 (2007).
59. J. L. De Bleecker *et al.*, 205th ENMC International Workshop: Pathology diagnosis of idiopathic inflammatory myopathies part II 28-30 March 2014, Naarden, The Netherlands. *Neuromuscular disorders : NMD* **25**, 268-272 (2015).
60. D. U. Kemaladewi *et al.*, Dual exon skipping in myostatin and dystrophin for Duchenne muscular dystrophy. *BMC Med Genomics* **4**, 36-36 (2011).

61. E. van der Wal *et al.*, Generation of genetically matched hiPSC lines from two mosaic facioscapulohumeral dystrophy type 1 patients. *Stem Cell Research* **40**, 101560 (2019).
62. A. Iuliano *et al.*, Coupling 3D Printing and Novel Replica Molding for In House Fabrication of Skeletal Muscle Tissue Engineering Devices. *Advanced Materials Technologies* **5**, 2000344 (2020).
63. S. Davis *et al.*, Expanding Proteome Coverage with CHarge Ordered Parallel Ion aNalysis (CHOPIN) Combined with Broad Specificity Proteolysis. *Journal of Proteome Research* **16**, 1288-1299 (2017).
64. F. D. W. Radstake, E. A. L. Raaijmakers, R. Luttge, S. Zinger, J. P. Frimat, CALIMA: The semi-automated open-source calcium imaging analyzer. *Computer Methods and Programs in Biomedicine* **179**, 104991 (2019).
65. M. I. Love, W. Huber, S. Anders, Moderated estimation of fold change and dispersion for RNA-seq data with DESeq2. *Genome Biology* **15**, 550 (2014).
66. Y. Perez-Riverol *et al.*, The PRIDE database and related tools and resources in 2019: improving support for quantification data. *Nucleic acids research* **47**, D442-d450 (2019).
67. R. Edgar, M. Domrachev, A. E. Lash, Gene Expression Omnibus: NCBI gene expression and hybridization array data repository. *Nucleic acids research* **30**, 207-210 (2002).

Supplementary Materials for

USP18 is an essential regulator of muscle cell differentiation and maturation

Cyriel Sebastiaan Olie[1], Adán Pinto-Fernández[2,3], Andreas Damianou[2,3], Salma el Abdellaoui[1], Iolanda Vendrell[2,3], Hailiang Mei[4], Bianca den Hamer[1], Erik van der Wal[1], Jessica C. de Greef[1], Anneke J. van der Kooi[5] ,Joost Raaphorst[5], Eleonora Aronica[6], Vered Raz[1*] and Benedikt M. Kessler[2,3]

* Corresponding author. Email: v.raz@lumc.nl

This PDF file includes:

Supplementary Text

Figs. S1 to S7

Tables S1 to S4

Fig. S1

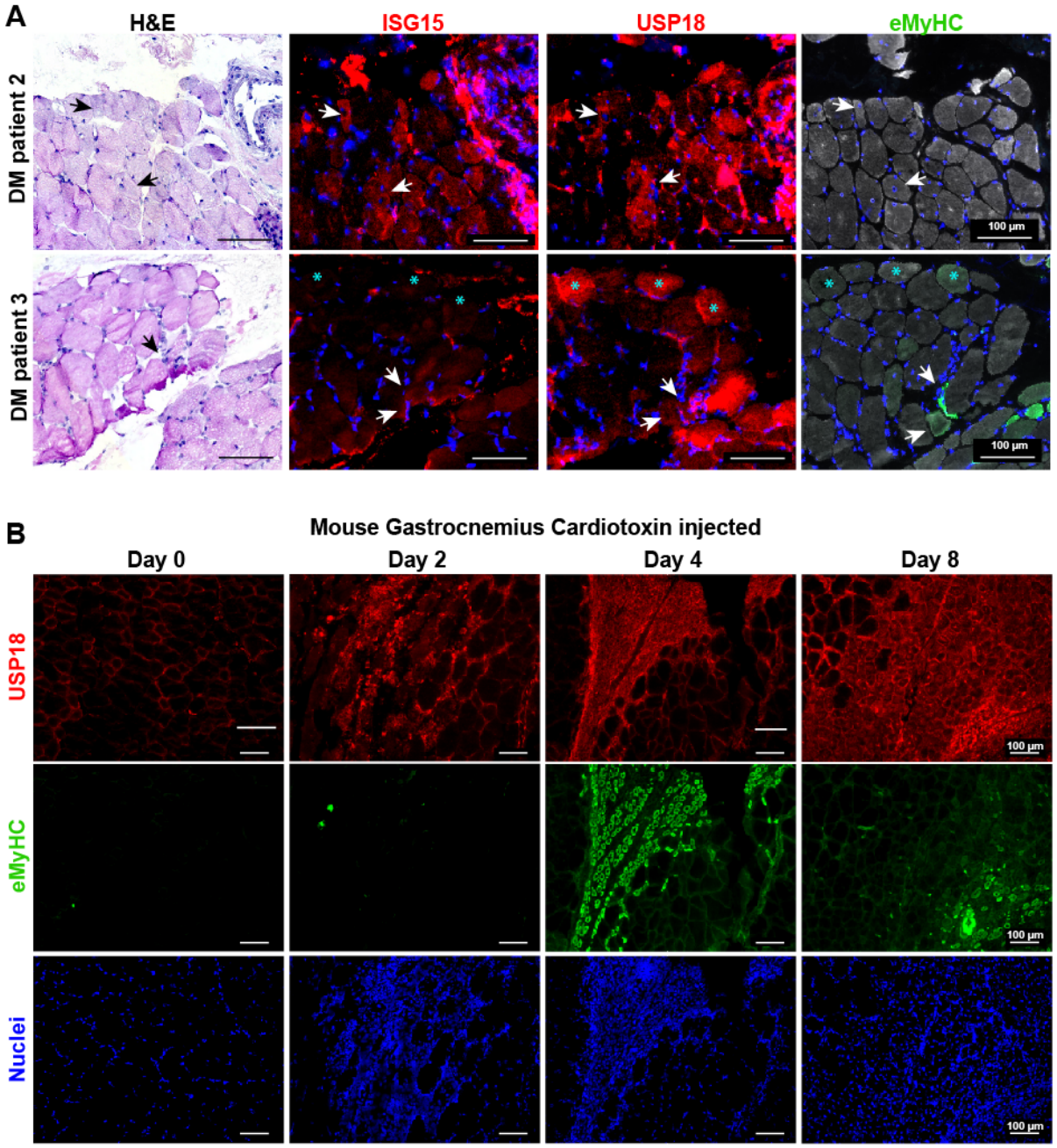

Figure S1. USP18 staining in DM patients and mouse tissues. (**A**) Human muscle from two dermatomyositis patients stained for H&E (1 & 5), ISG15 (2 & 6), USP18 (3 & 7) or eMyHC (4 & 8). Staining was performed on sequential cryosections where USP18 and ISG15 are presented in red and eMyHC in green, grey shows fluorescent background. Arrows in both patients indicate regeneration myofibers (centrally nucleated or eMyHC positive). Scale bars are 100 µm. (**B**) Images of each staining separately (USP18, eMyHC and nuclear staining) of the merged image in Fig. 1C. Scale bar is 100 µm.

Fig. S2

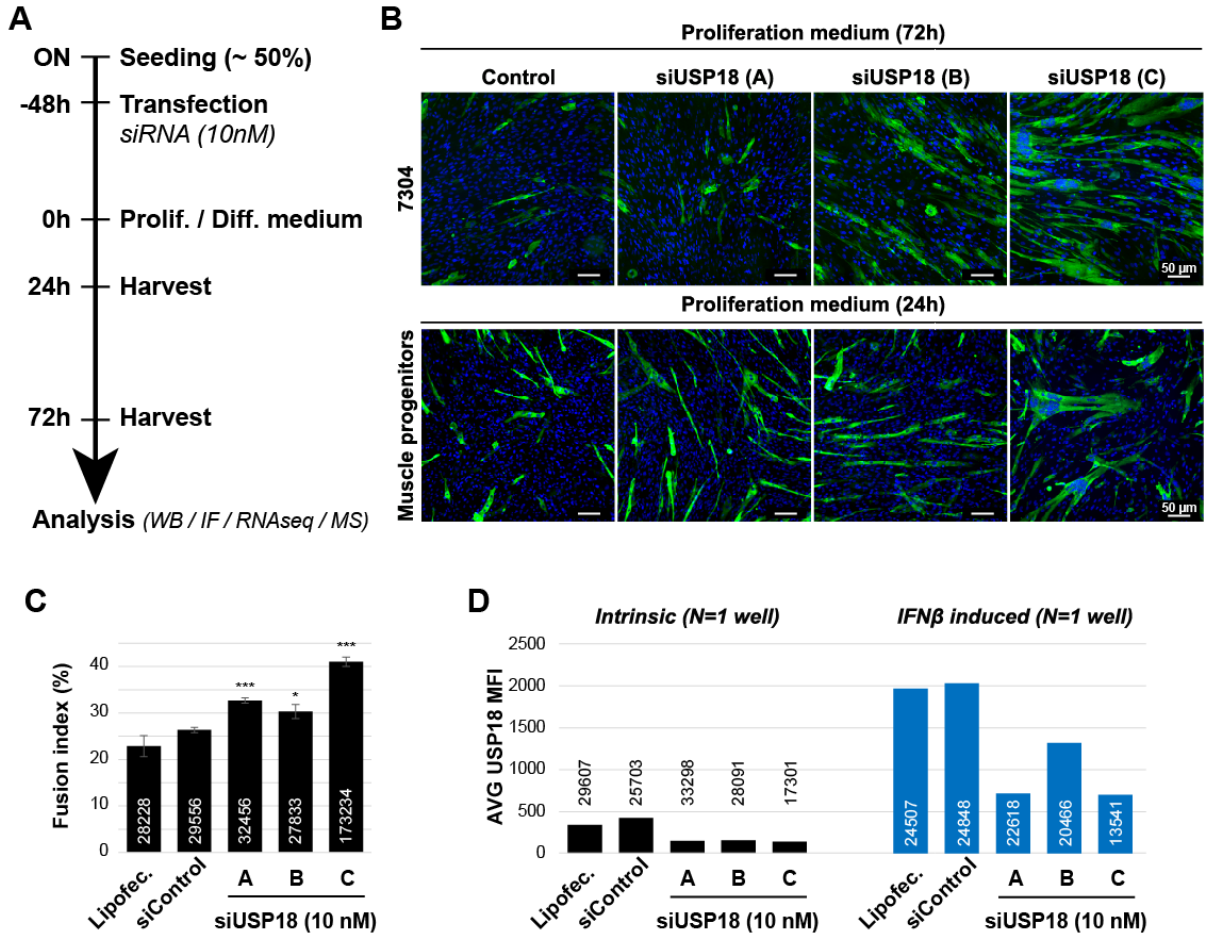

Figure S2. USP18 siRNAs reduce USP18 expression and induce premature differentiation. (**A**) A schematic overview of USP18 KD experimental setup. ON = overnight. All experiments were performed in at least three biological replicates. (**B**) Representative immunofluorescence images show MyHC staining after transfection of three USP18 siRNAs. Upper panel shows the effect after 72 hours in proliferation medium for 7304.1 muscle cells. Lower panel after 24 hours in proliferation for myogenic progenitor cells. Nuclei are coloured in blue. Scale bar is 50 µm. (**C-D**) Bar charts show the fusion index (C) and the respective USP18 mean fluorescence intensity (MFI) (D). USP18 MFI was measured from untreated or IFNβ-treated cell cultures (D). Number of cells is above/inside the bars. In panel C, average and error bars (SD) are from N=3. Statistical significance is depicted by asterisks. (*: 0.05-0.005, **: 0.005-0.0005, *** <0.0005). Panel D was average MFI over the indicated number of cells of one well.

Fig. S3

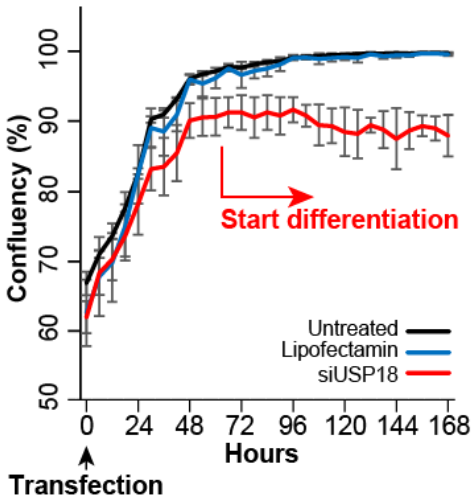

Figure S3. USP18 depletion stops cell growth. Graph shows a change in cellular confluency (%) in USP18 KD cells cultured in proliferation medium. Untreated, treated with transfection reagent only or transfected with siUSP18 are depicted with black, blue and red lines, respectively. Cell confluency was measured at 6h intervals and error bars show standard deviation over N=3 biological replicates. In panel B and E, the statistical significance is indicated by asterisks. (*: 0.05-0.005, **: 0.005-0.0005, *** <0.0005).

Fig. S4

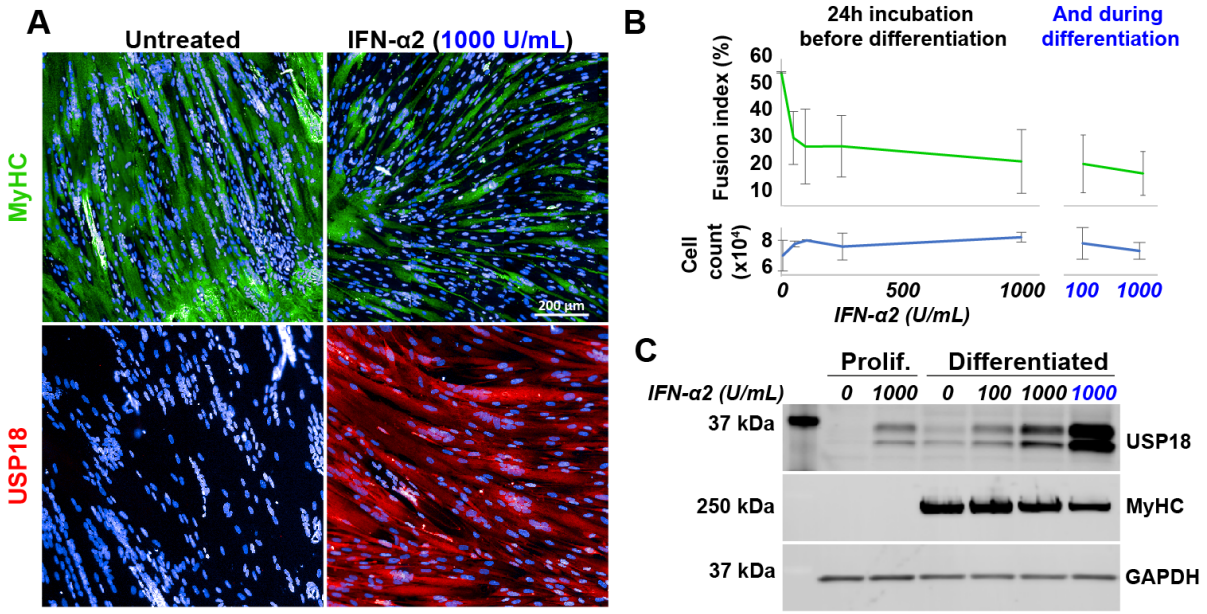

Figure S4. Excessive USP18 expression reduces muscle cell differentiation. (**A-C**) Different concentrations (U/mL) of IFN-2α were added in proliferation medium for 24h to the cultures, after which, proliferation medium was changed for differentiation medium that contained the same IFN-2α concentration, depicted with in blue, or without IFN-2α (black). Differentiation was carried out for 72h. (**A**) Representative immunofluorescence images show MyHC (green), USP18 (red) and nuclei (blue) staining. Scale bar is 200 µm. (**B**) Line plot shows the fusion index (green) for cell cultures treated with increasing IFN-2α concentrations. Blue line shows average number of nuclei from which the fusion index was calculated. Average and error bars (SD) are from N=2. (**C**) A representative western blot shows USP18 and MyHC expression for different IFN-2α concentrations. GAPDH was used as loading control.

Fig. S5

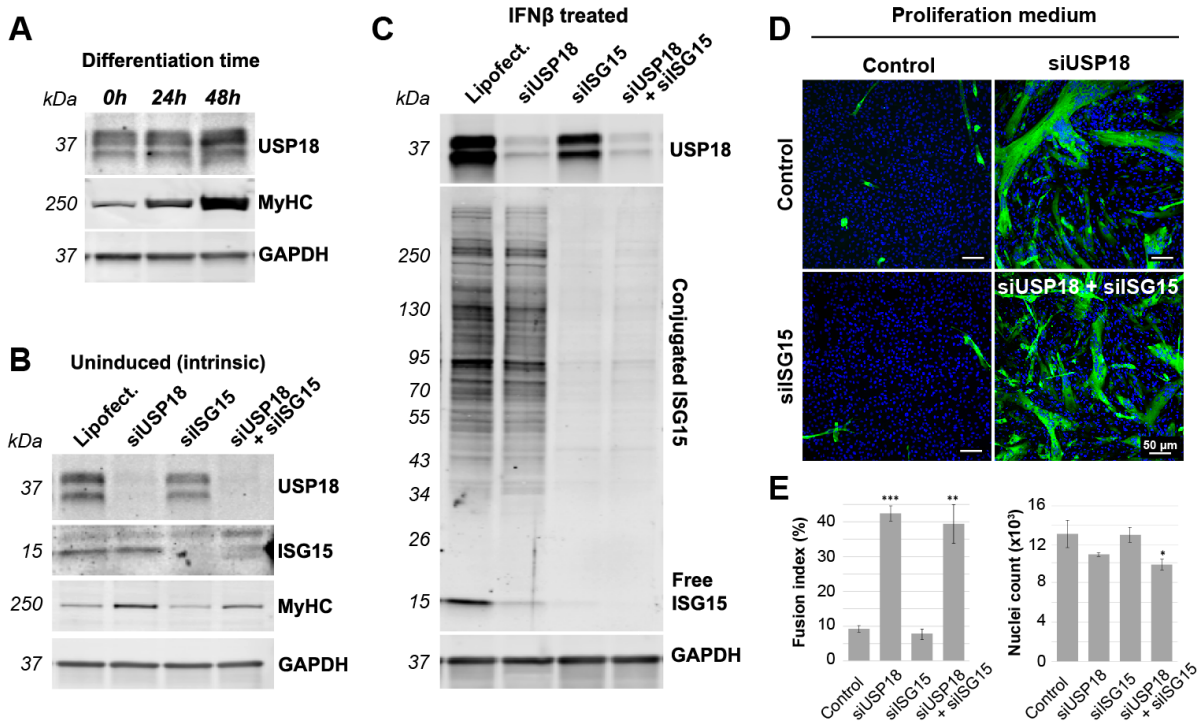

Figure S5. USP18 KD induces differentiation reprograming in myogenic progenitors. (**A**) Representative western blot shows USP18 and MyHC expression during differentiation. GAPDH indicates equal loading. (**B-C**) Representative western blots show USP18 and ISG15 expression. MyHC marks differentiation and GAPDH is a loading control. Panel B shows intrinsic (uninduced) protein expression and panel C shows expression after IFN-1 induction. (**D**) Representative immunofluorescence images show differentiating cells in siUSP18 cultures and co-transfection with siISG15 in proliferation medium. Scale bar is 50 µm. (**E**) Bar charts show fusion index and the respective cell count. Average and error bars (SD) are from N=3 biological replicates. Statistical significance is depicted by asterisks. (*: 0.05-0.005, **: 0.005-0.0005, *** <0.0005).

Fig. S6

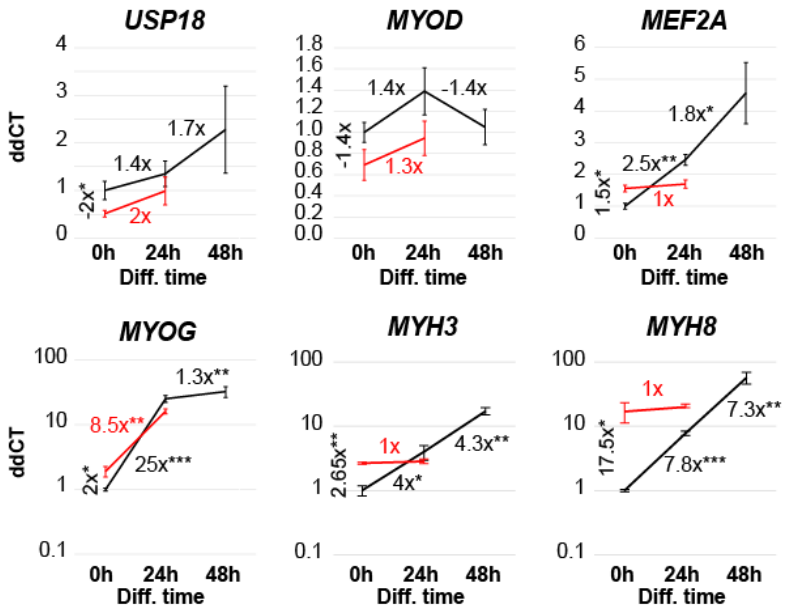

Figure S6. USP18 KD re-programs the myogenic regulatory factors profile, RT-qPCR validation. Graphs show the average ddCT values for differentiation in control (black) and USP18 KD (red) cell cultures. Average and error bars (SD) are from N=3. Statistical significance is depicted by asterisks. (*: 0.05-0.005, **: 0.005-0.0005, *** <0.0005).

Fig. S7

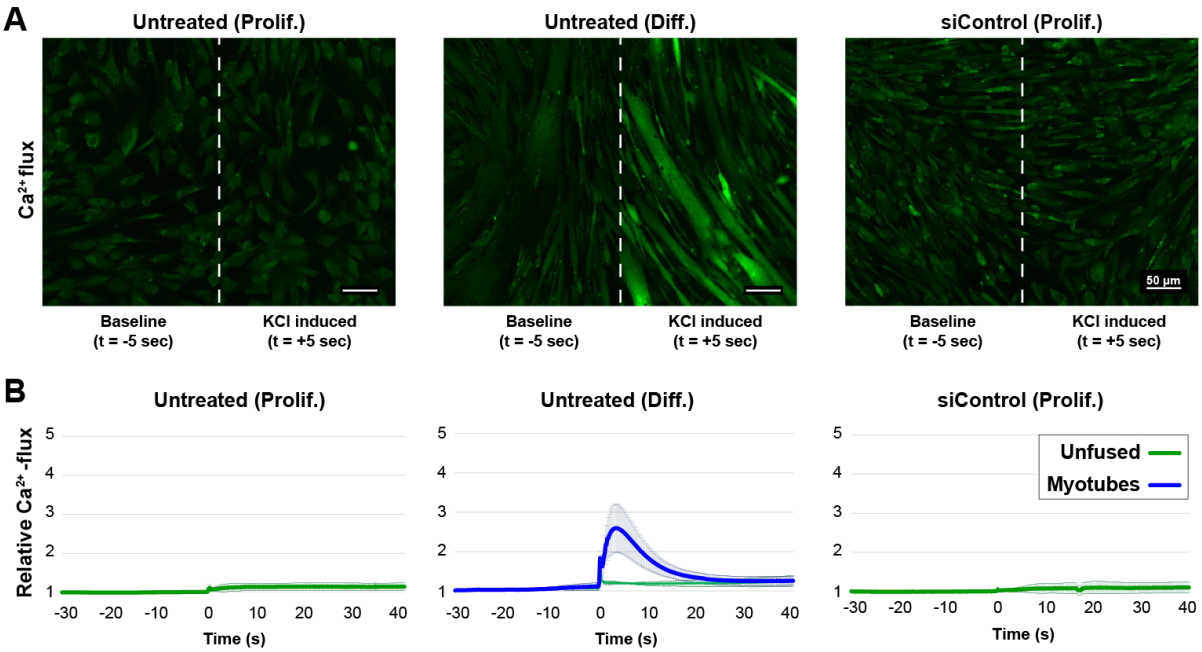

Figure S7. Calcium flux for proliferating and differentiating cells. (**A**) Representative images show the calcium flux (green signal) 5 seconds before or after KCl (10 mM) administration in control cells cultured in proliferation or differentiation medium. The respective images are separated by a white dashed line. Scale bar is 50 µm. (**B**) Graphs show the change in calcium flux over time. Calcium flux in uni-nucleated (unfused) or multi-nucleated (myotubes) cells is depicted by green or blue lines. Average and error bars (SD) are from N=3 biological replicates.

Table S1.

	Protein	Dilution		Host	Supplier	Cat. number
		IF	WB			
Primary antibodies	USP18	1:100	1:1000	anti-Rabbit	Cell signaling	#4813
	ISG15	1:100	1:1000	anti-Rabbit	Cell signaling	#2743
	pSTAT1	-	1:1000	anti-Rabbit	Cell signaling	#9167
	GAPDH	-	1:5000	anti-Mouse	Invitrogen	MA5-15738
	KLHL31	-	1:1000	anti-Rabbit	ProteinTech	24781-1-AP
	TNNI1	-	1:1000	anti-Rabbit	Novus Biologicals	NBP1-56641
	MyHC	1:250	1:250	anti-Mouse	DSHB	MF20
	TNNT3	-	1:1000	anti-Mouse	DSHB	JLT12
	eMYH3	1:100	-	anti-Mouse	DSHB	BF-45
	TTN	1:50	-	anti-Mouse	DSHB	9D10

	Target	Fluorophore	Dil.	Supplier
2nd antibodies	Anti-Rabbit	Cy5	1:5000	Thermo Fisher Scientific
	Anti-Mouse (IgG or IgM)	488	1:5000	Thermo Fisher Scientific
	WB anti-Rb/M	800/680	1:10000	IRDye 800CW or IRDye 680RD (LI-COR)

Table S1. List of used antibodies for immunofluorescence and western blotting.

Table S2.

siRNA	Supplier	Cat. number / sequence
Scrambled	Santa Cruz	sc-37007
siGenome	Dharmacon	#D-001206-13
USP18 (A)	Eurofins	CUGCAUAUCUUCUGGUUUA
USP18 (B)	Eurofins	GGAAGAAGACAGCAACAUG
USP18 (C)	Thermo Fisher	AM16708, ID: 105194
ISG15	Dharmacon	#L-004235-03-0005

Table S2. List of used siRNAs

Table S3. The USP18-dependent Transcriptome. Related to Fig. 3A-B and Fig. 4

Table S4. The USP18-dependent Proteome. Related to Fig. 5